DEVELOPING A QUALITY-CONTROLLED POSTGLACIAL SEA-LEVEL DATABASE FOR COASTAL LOUISIANA TO ASSESS CONFLICTING HYPOTHESES OF GULF COAST SEA-LEVEL CHANGE

A THESIS

SUBMITTED ON THE DECEMBER THIRD 2010

TO THE DEPARTMENT OF EARTH AND ENVIRONMENTAL SCIENCES

IN PARTIAL FULFILLMENT OF THE REQUIREMENTS

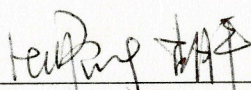OF THE SCHOOL OF SCIENCE AND ENGINEERING
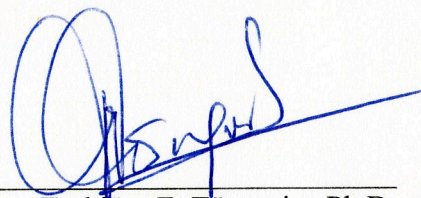
OF TULANE UNIVERSITY

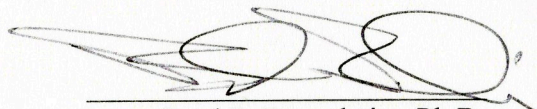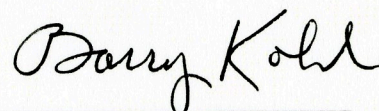FOR THE DEGREE

OF

MASTER OF SCIENCE

BY

_____
Ping Hu

APPROVED: _____
Torbjörn E. Törnqvist, Ph.D.

_____
Brad E. Rosenheim, Ph.D.

_____
Barry Kohl, Ph.D.

Abstract

A sea-level database following a new protocol of quality evaluation standards has been constructed and is used for a comparative analysis to reconcile conflicting hypotheses about Holocene relative sea-level change in the Gulf of Mexico.

Sea-level data are assessed quantitatively by assigning errors to both sample elevation and radiocarbon age. Sources of elevation uncertainty include sample thickness, indicative range, sampling errors, and surveying errors. Radiocarbon ages are corrected for bulk peat contamination, reservoir effects, and isotopic fractionation. Error calculations are performed as conservatively as possible. Furthermore, other variables such as sediment compaction are considered, in part relying on descriptive and semi-quantitative information that can prove useful for future studies. Overall, this database is valuable as a guideline for sea-level database standardization.

A relative sea-level database has been compiled for coastal Louisiana following the proposed protocol. Comparing relative sea-level records from the Mississippi Delta and the southwest Louisiana Chenier Plain reveals that local sea-level change in both areas exhibits the same trend. This result challenges a recent model used to reconcile the smooth trend of rising sea level in the Mississippi Delta with a mid-Holocene highstand elsewhere along the US Gulf Coast, which advocated cyclic uplift and subsidence of the Mississippi Delta caused by sediment excavation and filling of the Lower Mississippi Valley, respectively. Therefore, it is concluded that vertical crustal movements in coastal Louisiana (i.e., subsidence) are mainly controlled by glacio-isostasy, associated with the melting of the Laurentide Ice Sheet.

DEVELOPING A QUALITY-CONTROLLED POSTGLACIAL SEA-LEVEL DATABASE FOR COASTAL LOUISIANA TO ASSESS CONFLICTING HYPOTHESES OF GULF COAST SEA-LEVEL CHANGE

A THESIS

SUBMITTED ON THE DECEMBER THIRD 2010

TO THE DEPARTMENT OF EARTH AND ENVIRONMENTAL SCIENCES

IN PARTIAL FULFILLMENT OF THE REQUIREMENTS

OF THE SCHOOL OF SCIENCE AND ENGINEERING

OF TULANE UNIVERSITY

FOR THE DEGREE

OF

MASTER OF SCIENCE

BY

_____

Ping Hu

APPROVED: _____
Torbjörn E. Törnqvist, Ph.D.

_____
Brad E. Rosenheim, Ph.D.

_____
Barry Kohl, Ph.D.

Acknowledgement

I would first like to thank my advisor Dr. Torbjörn Törnqvist, who guided me to start the sea-level research and helped me to finish this master's thesis project. Tor is the most rigorous and patient teacher I have ever had. His confidence in me and always-there-help makes my today's accomplishment. I would also like to thank my committee members, Dr. Brad Rosenheim and Dr. Barry Kohl. Brad and Barry are like my other two advisors, providing me advice and comments with their expertise whenever they are needed. A debt of thanks must also go to Dr. Ben Horton and Dr. Simon Engelhart for their constructive comments and suggestions.

As colleagues working on different parts of the sea-level database project, Dr. Shiyong Yu and Dr. Juan González deserve the credits for sharing invaluable ideas and experience. I also want to thank Armin Straub for helping resolving some math issues.

I acknowledge the department of Earth and Environmental Sciences and the School of Science and Engineering at Tulane University for providing graduate students different resources in research such as teaching/research assistantship and travel grants for conferences, and in student life such as Educational Resources and Counseling (ERC). I particularly thank Ms. Ann Abrrecht at Tulane ERC for helping me going through a hard time.

I wish to thank my parents for their encouragements whenever I feel down. And whenever the support from the other side of the globe is not enough to cheer me up, Yige Zhang, my significant other, is always there with me. My other support system is from friendships. Zhixiong Shen, Chong "Carol" Chen, Kim Roe, Jianwei Han, Heng Wang, and Ningfang Yang are the most supporting friends I have ever had.

Finally, I would like to thank myself for not giving things up and working through the finish line.

Table of Contents

List of Symbols

A_0 Original (pre-disintegration) ^{14}C activity of a sample [Bq]

A_{on} Normalized ^{14}C activity of a standard [Bq]

A_s ^{14}C activity of a sample [Bq]

A_{sn} Normalized ^{14}C activity of a sample [Bq]

A_t ^{14}C activity of a sample at time t [Bq]

Age_c ^{14}C age after analytical, bulk, reservoir, and isotopic fractionation correction [^{14}C yr]

D_a Apparent sample depth due to non-vertical drilling [m]

D_t True sample depth [m]

E_a Analytical error of ^{14}C measurement [^{14}C yr]

E_b Bulk error of ^{14}C measurement [^{14}C yr]

E_I Isotopic fractionation error for samples without evidence that isotopic fractionation correction has been performed [^{14}C yr]

E_i Error of isotopic fractionation correction [^{14}C yr]

E_{ir} Error of indicative range [m]

E_{ls} Error of land surface surveying [m]

E_{nv} Error of non-vertical drilling [m]

E_r Reservoir error [^{14}C yr]

E_s Error of sampling [m]

E_{ta} Total age error [^{14}C yr]

E_{te} Total elevation error [m]

H_{ir} Indicative range [m]

H_{RWL} Height of reference water level [m]

H_{RSL} Height of relative sea level [m]

H_s Sample elevation [m]

N Number of remnant ^{14}C atoms

N_0 Number of original ^{14}C atoms before decay

t Decay time or the ^{14}C age [^{14}C yr]

t_m Measured ^{14}C age without correction [^{14}C yr]

t_n Normalized ^{14}C age for isotopic fractionation [^{14}C yr]

T Sample thickness [m]

T_d Decompacted sample thickness [m]

U_{te} Total elevation uncertainty [m]

ΔR Reservoir age correction [^{14}C yr]

Δt_i Isotopic fractionation correction [^{14}C yr]

θ Borehole angle with respect to the vertical [degree (°)]

λ Decay constant

σ Standard deviation of ^{14}C measurement [^{14}C yr]

Chapter 1 Introduction

1.1 Sea-Level Research History along the US Gulf Coast

A large body of work has been carried out across the world since sea-level change drew

the attention of geologists in the 1950s as part of the puzzle of paleoclimatology and

paleoceanography. After the attempts to reconstruct a purely eustatic sea-level curve

since the Last Glacial Maximum (LGM), sea-level researchers found that sea-level curves

from different geographic areas are affected significantly by regional or local effects such

as tectonic movements of the crust, compaction of sediments, isostatic uplift and

subsidence in response to waning and waxing ice sheets, and so on. Therefore, it is

difficult to distinguish the purely eustatic sea-level change from other factors. As a result,

since the 1970s geologists have focused primarily on regional or local sea-level changes,

rather than eustasy (Van de Plassche, 1986; Pirazzoli, 1991; Milne and Mitrovica, 2008).

The Gulf of Mexico is known as one of the earliest natural laboratories of sea-level

research and continues to attract considerable interest today. Two main scenarios of

Holocene sea-level change along the US Gulf Coast have been under debate for the past

50 years. One postulates that sea level continuously rose from about -10 m to the present

level during the last 8000 years or so, based mainly on sea-level indicators from

subsurface coastal strata (e.g., Gould and McFarlan, 1959; Curray, 1961; McFarlan, 1961;

Coleman and Smith, 1964; Scholl and Stuiver, 1967; Nelson and Bray, 1970; Frazier,

1974). The alternative view advocates that sea level rose to as much as 2 m above the present level during the middle to late Holocene and then dropped to the present level, as inferred from elevated beach-ridge deposits (e.g., Behrens, 1966; Tanner et al., 1989; Stapor et al., 1991). Morton et al. (2000) and Blum et al. (2001) revitalized the mid-Holocene highstand hypothesis, using beach ridges with subtidal faunal assemblages to infer a relative sea-level (RSL) highstand of up to 1.95 m during 6800 – 4800 cal yr BP (Blum et al., 2001) and RSL fluctuations of ±1.5 m from 5500 to 1200 cal yr BP (Morton et al., 2000). Törnqvist et al. (2004a) subsequently published a detailed RSL curve, using basal peat from the Mississippi Delta, to track sea-level change from 8000 to 3000 cal yr BP. They argued that RSL rise during this time interval followed a relatively smooth rising trend, without highstands. This RSL curve was then extended into the present by Törnqvist et al. (2006) and González and Törnqvist (2009) and used to argue that the Pleistocene substrate underneath the Mississippi Delta subsides at a rate of only a fraction of a millimeter per year. However, Blum et al. (2008) questioned this by proposing an "ups and downs" model of cyclic uplift and subsidence with a magnitude of at least 9 m along the paleovalley margins underneath the Mississippi Delta. They argued that this was caused by the excavation and filling of sediment in the Lower Mississippi Valley, with incision during the LGM followed by valley filling and delta construction during the Holocene sea-level rise. Resolving this long-standing debate is the initial motivation for this thesis.

1.2 Need for a Standardized Sea-Level Database

The difficulty in reconciling the two hypotheses outlined above is partly due to the fact that the different patterns of RSL change are based on different types of sea-level indicators and their quality is often not rigorously assessed based on a uniform standard. Furthermore, many studies simply plot sea-level data points to construct a RSL curve without taking into account the elevation and age uncertainties introduced by sampling and other factors (e.g., sediment compaction, reservoir and isotopic fractionation effects) which could lead to different interpretations. Thus, before any comparative analysis is performed with different types of sea-level indicators from different locations, a standardized sea-level database is needed.

A long history exists of the construction of sea-level databases for specific geographic areas (e.g., Shennan, 1989; Shennan et al., 2000a; Shennan and Horton, 2002; Shennan et al., 2002; Simms et al., 2007; Engelhart, 2010). In these studies, the age error is typically the analytical error reported by the radiocarbon dating laboratory; the elevation error is the sum of a variety of errors such as those associated with field leveling, tide levels, and the indicative range (Shennan et al., 2000a; Shennan and Horton, 2002). These studies have established the foundation for constructing standardized sea-level databases on which this thesis builds. However, additional sources of error need to be examined to make different types of sea-level indicators comparable to each other.

1.3 Objectives

This thesis aims to establish a quality-assessed Holocene sea-level database for coastal

Louisiana by reevaluating published data and quantifying all potential errors as

cautiously as possible for both elevation and age. This database will then be used to test

the two competing hypotheses of RSL change along the Gulf Coast during the Holocene.

In other words, the new sea-level database will be used to determine whether sea level

has been continuously rising to the present level or whether there were one or more

sea-level highstands.

Chapter 2 Database Protocol

Sea-level data used to reconstruct Holocene RSL change in coastal Louisiana are

assessed quantitatively by assigning errors to their elevation and age, as well as tabulating

other relevant information such as the location of sampling sites, the nature of

radiocarbon dated material, the stratigraphic context, and so on, as derived from

published studies. This chapter lays out a detailed protocol for sea-level database

construction in coastal Louisiana and elsewhere.

2.1 Sea-Level Index Points and Limiting Data Points

Age-depth data that are used in sea-level reconstructions include sea-level index points

and limiting data points, based on whether or not they have a well constrained indicative

meaning with respect to a tide level.

2.1.1. Sea-Level Index Points

Sea-level index points have a well-defined indicative meaning which includes the

relationship of the sea-level indicator to a tide level plus an indicative range. The

indicative meaning is defined by Van de Plassche (1986) as "expressed in terms of the

indicator, or a relevant or convenient aspect thereof, and a vertical range with respect to

that indicator or aspect, above, below or within which the reference water level occurs or

occurred given the water-level relationship of the indicator". The vertical range is
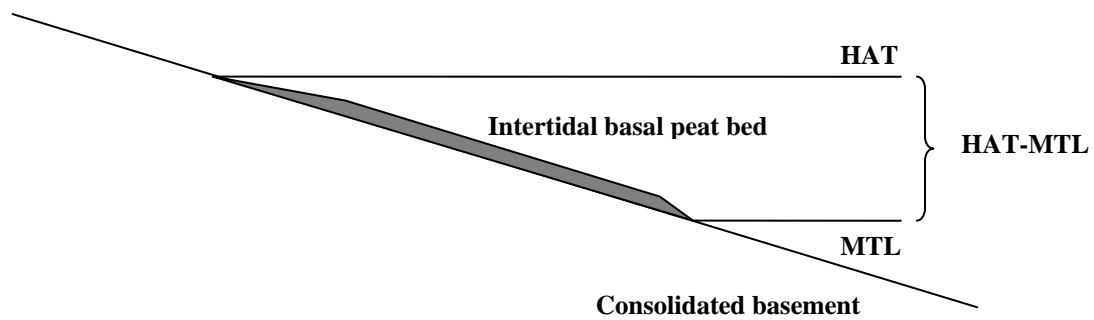
Figure 1. Illustration of the indicative meaning of intertidal basal peat that formed above mean tide level (MTL) and below the highest astronomical tide (HAT). Past mean sea level should be within the interval of the half tidal range as measured below the basal-peat sample. Two end members can be distinguished, where either the basal peat formed exactly at MTL and its elevation represents the past mean sea level or the past mean sea level was at an elevation of a half tidal range below the basal peat if the basal peat formed at HAT.

referred to as the indicative range (Van de Plassche, 1986). Examples of sea-level

indicators include intertidal marsh peat and plant macrofossils and/or charcoal fragments

within it. This intertidal peat formed anywhere between mean sea level (MSL,

approximated by the closely related mean tide level, MTL) and the spring high tide level

(represented by the level of the highest astronomical tide, HAT) (Engelhart, 2010) (Fig.

1). Accordingly, the past mean sea level suggested by this type of sea-level indicator can

be located within the half tidal range below the elevation of the peat sample. Unlike the

classification of coastal peat deposits along the US Atlantic Coast into several categories

(e.g., high marsh versus low marsh; Engelhart, 2010), peat along the US Gulf Coast is

classified into intertidal peat and freshwater peat associated with the smaller tidal range.

These two categories then are used as index points and upper limiting data, respectively.

2.1.2. Limiting Data Points

Limiting data points do not have a specific indicative range relative to a reference water

level. However, they can still provide useful information about past sea level, and define

its upper or lower limit with respect to a specific reference water level. There are two

types of limiting data points in the present sea-level database. Compaction-free

freshwater peat in coastal areas is thought to have formed above the mean tide level.

Therefore, it can serve as an upper limiting data point, indicating that past sea level must

have occurred at the same or a lower level. In contrast, *in situ* marine mollusk shells can

be used as lower limiting data points indicating that past mean sea level was somewhere

at or above the elevation of their occurrence, provided that they live below the mean tide

Table 1. Mollusks from the central US Gulf Coast that are used in the sea-level database. Mollusk habitats, environmental information, and depth ranges are from Parker (1960), Andrews (1971), and B. Kohl (personal communication, 2010). Depth is with respect to the water surface, which is assumed to be mean sea level.

Class	Habitat		Taxon	Environment	Depth –min (m)	Depth – max (m)
Bivalve	Epifaunal	Attached epifaunal	*Crassostrea virginica*	Brackish bays and estuaries	0	
			Ostrea equestris	High-salinity oyster reef	0	
			Echinochama cornuta		18	110
			Plicatula gibbosa			
			Chama congregata			
		Free-living epifaunal	*Aequipecten gibbus*	Intermediate shelf	22	64
			Pecten sp.	Intermediate to outer shelf	22	
		Epifaunal byssate fissure dweller	*Lima scabra*	Offshore		
		Other	*Arca* sp.			
	Infaunal		*Rangia cuneata*	River-influenced areas	0	
			Mulinia lateralis	Prodelta slope	4	20
			Abra aequalis	Open sound, lagoon centers, near shore in clayey sediments		
			Phacoides sp.	Open-bay margins and hypersaline lagoons		
			Mercenaria	Off shore, open bay and inlet-influenced areas		
			Diplodonta	Inlet-influenced areas		
			Crassinella sp.	Inlet-influenced areas and channels on shelly bottom		
			Anadara transversa	Inlet-influenced areas and offshore	0	11
			Corbula swiftiana	Inlet-influenced areas, open-bay margins		
			Tellina	Inner shelf to intermediate shelf on sand bottom	4	64
			Dinocardium robustum	Inner shelf, close to the shore and in inlet-influenced areas	4	22
			Chione intapurpurea	Inner shelf, near shore	4	22
			Dosinia	Inner shelf, near shore		
			Varicorbula operculata	Off shore to intermediate shelf, mud bottom	37	73
			Nuculana sp.	Sandy mud bottom beyond low tide		
Gastropod			*Busycon* sp.	Brackish bays and estuaries	4	22
			Strombus sp.	Intertidal to about 10 fathoms	0	18

level. Both index points and limiting data points are useful only if it can be demonstrated that the samples have not been reworked and redeposited.

Table 1 lists mollusk genera (and species, if applicable) used as sea-level limiting data points in the sea-level database. It also lists the habitat information (i.e., living environment and depth range of occurrence) of these mollusks. The depth range may vary under different conditions controlled by factors such as water temperature, river discharge, turbidity, and so on (Parker, 1960). Due to this, depth ranges listed in this table are not reliable to serve as the indicative range. However, the more habitat information is known for each taxon, the more their depth range can be constrained and hence the more qualified the mollusks are to serve as "semi-index points" or, in the ideal case, as index points. Thus, as more information on modern mollusk distributions becomes available, this table can be updated and become more useful (B. Kohl, personal communication, 2010).

2.2 Geographic Location

The geographic location of all sea-level index points and limiting points in the database are converted from their original formats to decimal degrees of latitude/longitude. There are five types of original formats for location in this database: 1) latitude/longitude - decimal degrees; 2) latitude/longitude - degrees/minutes/seconds; 3) Universal Transverse Mercator (UTM) coordinates - Zone, North/East; 4) US Public Land Service (PLS) coordinates -Township/Range/Section (/Quadrant); and 5) descriptive locations. In

the converted format, decimals represent different levels of resolution of a location: 4, 3, 2, 1, and 0 decimals indicate a sampling site can be located within 10 m, 100 m, 1 km, 10 km, and 100 km, respectively, along latitudinal and longitudinal directions. No location resolution greater than 4 decimals is used in this database. The number of decimals in the final format is determined by the resolution, as provided by the original data source. In this sea-level database, all coordinates use the North and the East as default quadrants (following the protocol of Engelhart, 2010), thus west longitudes are converted to negative values. No conversion is needed when the original format is in decimal degrees. The original format of degree/minute/second is converted to decimal degrees by converting minutes and seconds to decimal degrees arithmetically. Conversion processes for the other three formats are clarified below in more detail.

The outdoor mapping program TOPO! 4.2 released by National Geographic was used to locate and convert UTM coordinates to decimal latitude/longitude degrees. This was done by plotting sampling sites on the TOPO! 4.2 map document using UTM coordinates and then choose the display format of location as geographic coordinates, i.e., latitude/longitude. For example, a series of sampling sites are plotted on a TOPO map document in Fig. 2A in the format of UTM coordinates using geodetic datum NAD 27. The displaying format of the same locations is converted to decimal degrees using geodetic datum NAD 83 in Fig. 2B.

Figure 2A. Location input in the format of UTM coordinates related to geodetic datum NAD 27; and B. Locations displayed in the format of decimal degrees related to geodetic datum NAD 83. Conversions are carried out with the "preference and settings" tool in TOPO! 4.2.

Most US states are covered by the PLS system that was introduced in the late 1700s. Exceptions include the original thirteen states, some areas in the southwestern US where land surveys may be based on Spanish land grants, and areas which were never surveyed (Higgins et al., 2009). As illustrated in Fig. 3, establishment of the PLS scheme in each state was started by surveying base lines, similar to latitudes, and principal meridians, similar to longitudes. Additional lines were then surveyed parallel to these and 6 miles apart in order to create grids of 6 mi × 6 mi. Rows parallel to the base line are called townships and columns parallel to the principal meridian are called ranges. Townships and ranges are labeled with number and direction relative to the base line and the principal meridian, respectively (e.g., Township 1 North, Township 2 South, Range 1 East, Range 2 West). Each township/range square is divided into 36 small (1 mi × 1 mi) sections, beginning from the upper right corner. Each section is divided into four quadrants (NE, SE, SW, and NW) and each quadrant can be subdivided into four quadrants which can be further subdivided. For example, point X in Fig. 3 is in the southeastern quadrant of the southeastern quadrant of the southwestern quadrant of the southeastern quadrant of section 11 in the square of Township 1 South and Range 2 West, which is expressed as SE1/4SE1/4SW1/4SE1/4 sec.11, T1S, R2W. The resolution of point X's location is as good as 100 m. Thus, its longitude and latitude are rounded to the third decimal.

Locations of sea-level data published during the 1950s and 1960s (e.g., Kulp et al., 1952; Broecker et al., 1956; Brannon et al., 1957; Broecker and Kulp, 1957; McFarlan, 1961)

6 miles

T2N

T1N

BASE MERIDIAN LINE (surveyed)

PRINCIPAL

T1S   Township
       T1S, R2W

6 miles

T2S

T3S

N

R5W R4W R3W R2W R1W R1E R2E R3E R4E R5E R6E

A. Township and range grid

6 miles

6	5	4	3	2	1
7	8	9	10	11 Section	12
18	17	16	15	14	13
19	20	21	22	23	24
30	29	28	27	26	25
31	32	33	34	35	36

T 1 S

6 miles

N

R 2 W

B. A township contains 36 sections

1 mile

NW   NE   N

11   1 mile

NW   NE

SW   Z•

SW   SE

X•

C. Sections are further subdivided
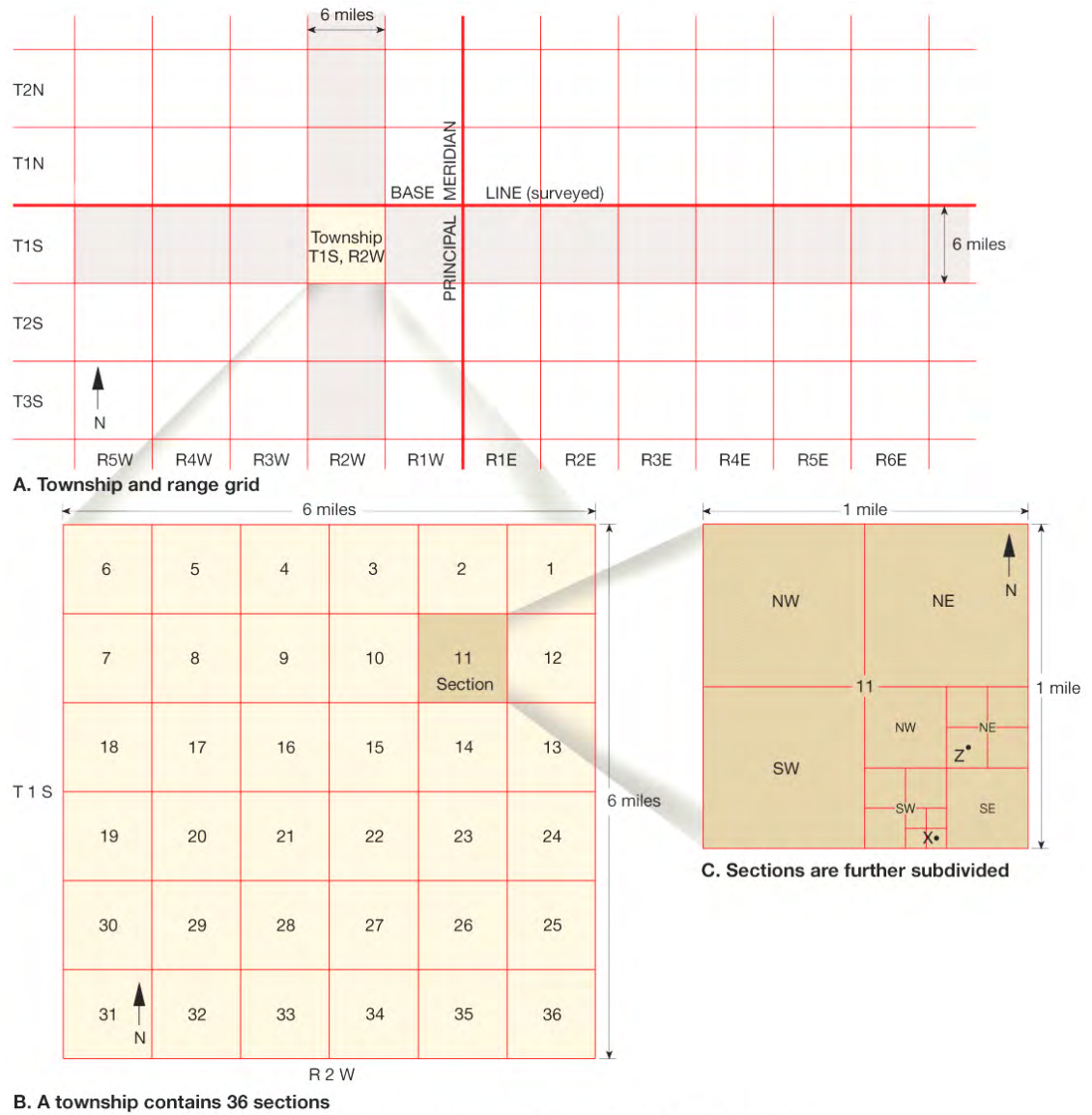
Copyright © 2006 Pearson Prentice Hall, Inc.

Figure 3. Illustration of the Public Land Service coordinate system (Higgins et al., 2009).

use PLS coordinates. Conversions are performed as follows. First, locations are found on topographic maps which include the PLS coordinate system (TOPO! 4.2) based on their PLS coordinates. Second, the "Waypoint Tool" is used to mark the location on the map and a name can be given to this point (I use laboratory code if available, otherwise the sample name). Location information is then displayed in the information sheet below the map, with latitudes and longitudes in the format of degrees/minutes. Decimal degrees are then obtained from the arithmetic conversion discussed above. For example, the original location of sample O-393 (McFarlan, 1961) was SW1/4, SW1/4, sec. 33, T11S, R1W. After it was found and marked by the "Waypoint Tool", the latitude and longitude of this location was displayed as 29º35.497' N and 92º29.017' W. The final converted location is 29.592º N, -92.484º E with 3 decimals because it can be located within a 400 m × 400 m square (Fig. 4).

Descriptive locations only provide general names of a study area. Sample sites can be roughly located based on the study area's name, using the "Place Finder Tool" in TOPO! 4.2. However, the resolution of the corrected latitude/longitude of locations can only be rounded to 1 or 0 decimals because areas found by names usually have a resolution of 10 to 100 km only. For example, a sampling site reported in Coleman and Smith (1964) is given as "Pecan Island, Louisiana". After inputting this name, TOPO! 4.2 returned two results of different types of information matching the query (Fig. 5). By double clicking either of the results, the software highlights the location on the map. Marking the location using "Waypoint Tool" and proceeding with the arithmetic conversion provides decimal
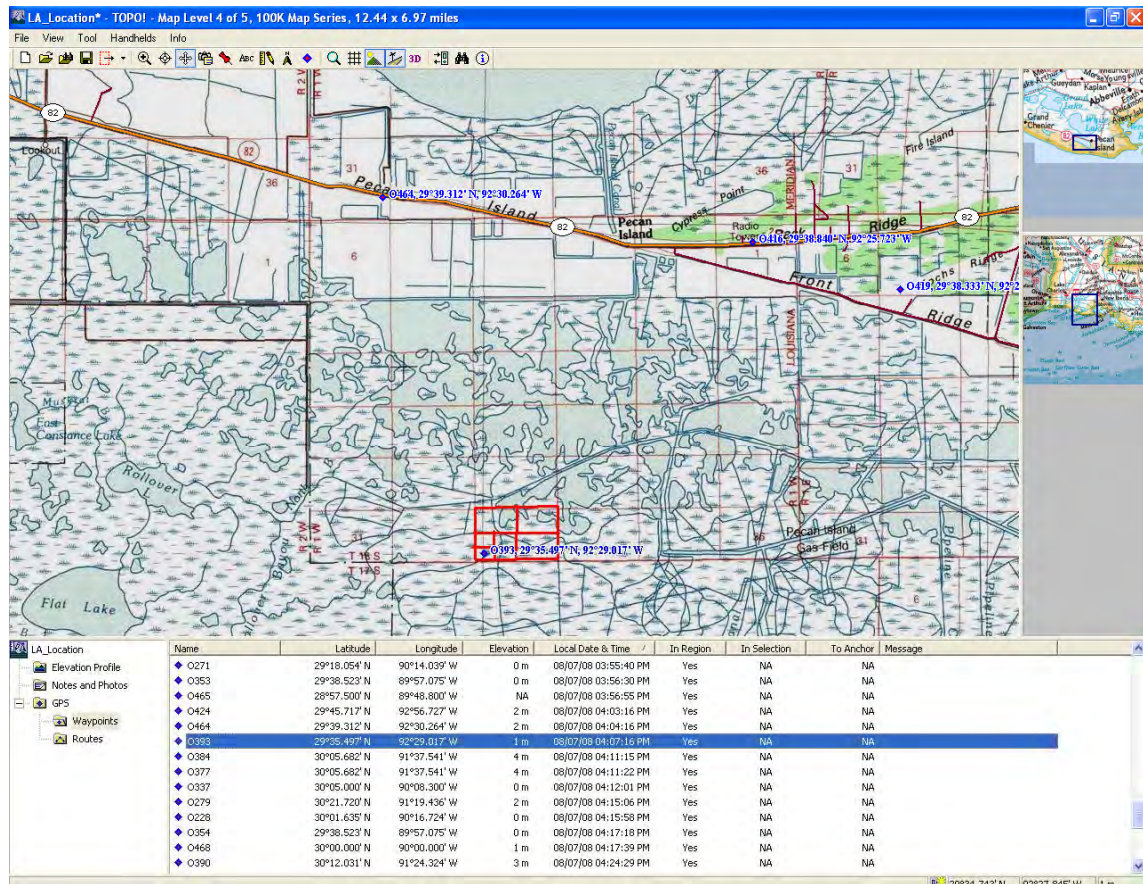
Figure 4. Locating sea-level data using the PLS coordinates on topographic maps and the Waypoint Tool in TOPO! 4.2.
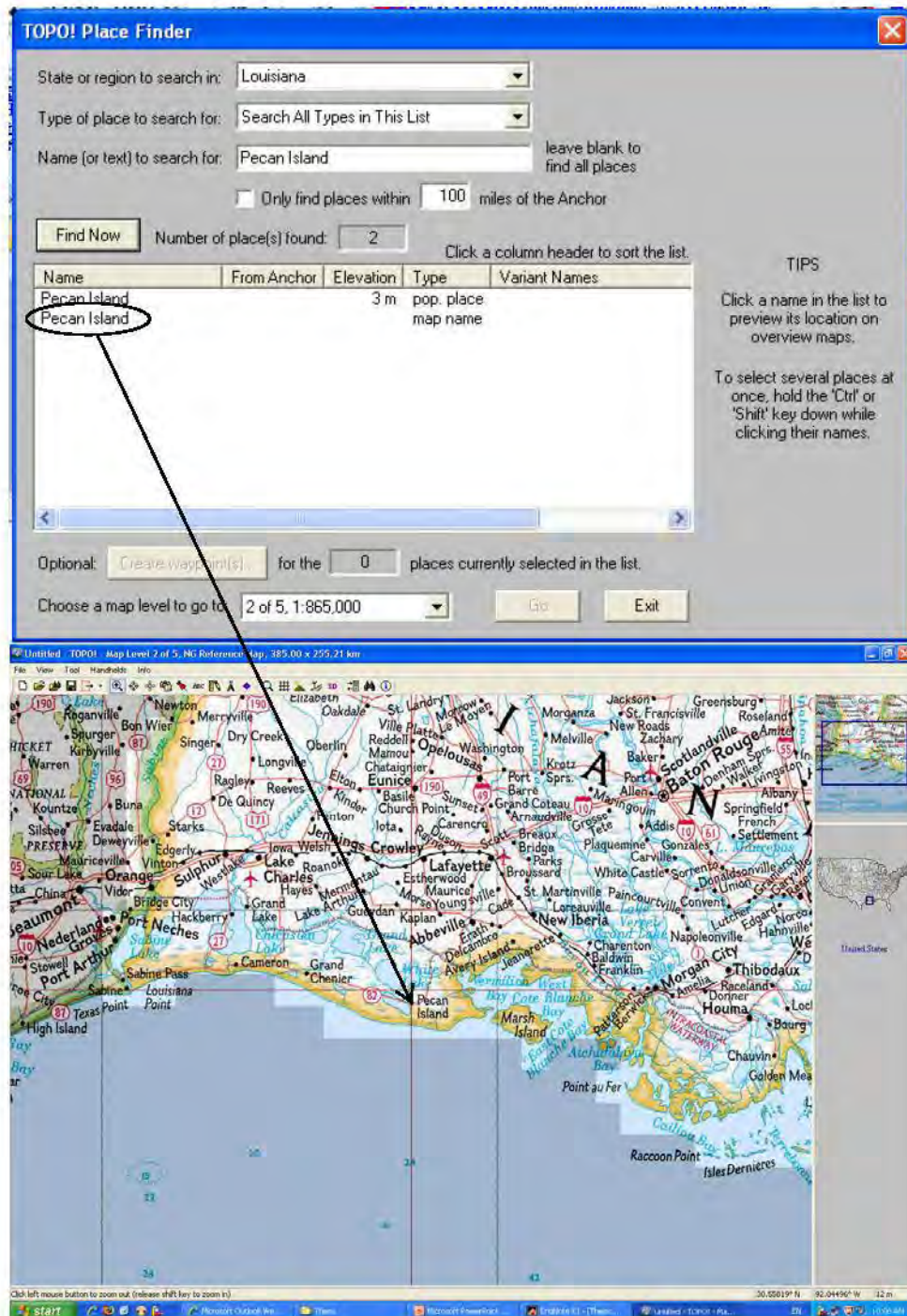
Figure 5. Locating study area by name of the area using Place Finder Tool in TOPO! 4.2.

degrees of latitude/longitude of 29.5° N, -92.5° E, rounded to 1 decimal, given that the

resolution in this case is about 10 km.

2.3 Elevation Uncertainty

The total elevation uncertainty in this study comprises sample thickness and a variety of

errors arising from the indicative meaning of sea-level indicators, sampling and land

surface surveying, among others (Fig. 6), expressed as the equation

$$U_{te} = T + 2 \cdot E_{te} \qquad [1]$$

in which U_{te} is total elevation uncertainty; T is the sample thickness (note that this may

involve a decompaction correction, as discussed in section 2.4); and E_{te} is the total

elevation error, expressed as

$$E_{te} = \sqrt{E_{ir}^{2} + E_{s}^{2} + E_{nv}^{2} + E_{ls}^{2}} \qquad [2]$$

in which E_{ir}, E_s, E_{nv} and E_{ls} represent indicative range error, sampling error, non-vertical

drilling error, and land surface surveying error, respectively. For example, a peat sample

that has $T = 2$ cm, $E_{ir} = \pm 15$ cm, $E_s = \pm 10$ cm, $E_{nv} = \pm 2$ cm and $E_{ls} = \pm 10$ cm, yields

$$E_{te} = \sqrt{(\pm 15)^{2} + (\pm 10)^{2} + (\pm 2) + (\pm 10)^{2}} = 20.71 \text{cm}$$

and $\qquad\qquad\qquad U_{te} = 2 + 2 \times 20.71 = 43.42$ cm
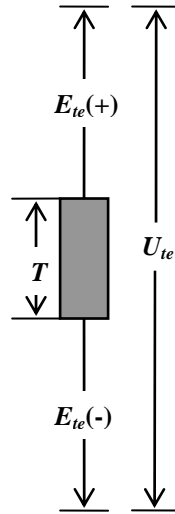
Figure 6. Illustration of the vertical uncertainty of a sea-level index point. U_{te} **is total elevation uncertainty;** T **is sample thickness; and** E_{te} **is total elevation error.**

2.3.1 Indicative Meaning

Sea-level indicators are featured with their indicative meaning relative to present or former sea level or sea-level influenced groundwater level. The indicative meaning of index points enables the reconstruction of past RSL, as follows (Shennan, 1982)

$$H_{RSL} = H_s - H_{RWL} \qquad [3]$$

where H_{RSL} represents the elevation of relative sea level, H_s represents sample elevation and H_{RWL} represents the elevation of the reference water level which the sample elevation is related to. Furthermore,

$$E_{ir} = H_{ir} / 2 \qquad [4]$$

where H_{ir} represents the indicative range.

In this thesis, three sea-level indicator categories are discussed, including: 1) intertidal marsh peat, 2) compaction-free freshwater peat, and 3) marine/estuarine carbonates (e.g., mollusk shells). Table 2 lists their reference water levels and indicative ranges, respectively. The open indicative range of freshwater peat and marine/estuarine carbonates implies that they can only be used as limiting data points.

Tide-gauge data to infer reference water levels are obtained from the NOAA tides and currents website. Unfortunately, no information is provided from NOAA tide gauges on the highest astronomical tide (HAT) along the Gulf Coast. As an alternative, I use 10 years of predictions provided by NOAA for each tide gauge and take the average of the highest predicted tide of each month as the annual HAT (Engelhart, 2010).

Table 2. Reference water level and indicative range of different types of sea-level indicators

Sea-level indicator	Reference water level	Indicative range
Intertidal marsh peat	(HAT+MTL)/2	HAT-MTL
Compaction-free freshwater peat	MTL	Anywhere at or above RWL
Marine/estuarine mollusks	MTL	Anywhere at or below RWL

HAT = highest astronomical tide; MTL = mean tide level; RWL = reference water level (following Engelhart, 2010).

2.3.2 Sample Thickness

Sample thickness defines the initial elevation uncertainty of sea-level index points with the consideration that several decimeters of vertical difference of sea-level indicators sometimes lead to distinct interpretations of patterns and rates of Holocene sea-level changes (Van de Plassche, 1986) and that thicknesses of samples sometimes can be on the order of meters (e.g., Broecker et al., 1956; Brannon et al., 1957; Broecker and Kulp, 1957; McFarlan, 1961; Coleman and Smith, 1964; Nelson and Bray, 1970; Frazier, 1974; Kulp, 2000). While sample thickness is reported for many published sea-level data, larger numbers of studies lack this information. In the former case, sample thickness is directly adopted from the original studies, while in the latter case estimations are made based on thicknesses reported by comparable studies.

Sample thickness varies among studies with respect to the necessary amount of sample for radiocarbon dating. Sample thickness of peat samples can be as little as a few centimeters (e.g., Törnqvist et al., 2004a, 2004b, 2006; González and Törnqvist, 2009) to a few decimeters (e.g., Milliken et al., 2008; J.B. Anderson, personal communication, 2010), and 2 cm for mollusk shell samples (Simms et al., 2007) using the accelerator mass spectrometry (AMS) ^{14}C dating technique. Thus, I assign 20 cm as sample thickness for AMS dated samples lacking thickness information. On the other hand, studies using conventional ^{14}C dating showed sample thicknesses of 0.3 - 6.5 m from cores and 3 - 12 m from cuttings (Broecker et al., 1956; Brannon et al., 1957; Broecker and Kulp, 1957; McFarlan, 1961; Coleman and Smith, 1964; Nelson and Bray, 1970; Frazier, 1974; Kulp,

A.   **Sample Thickness Distribution (Cores)**

B.   **Cumulative Distribution of Sample Thickness (Cores)**
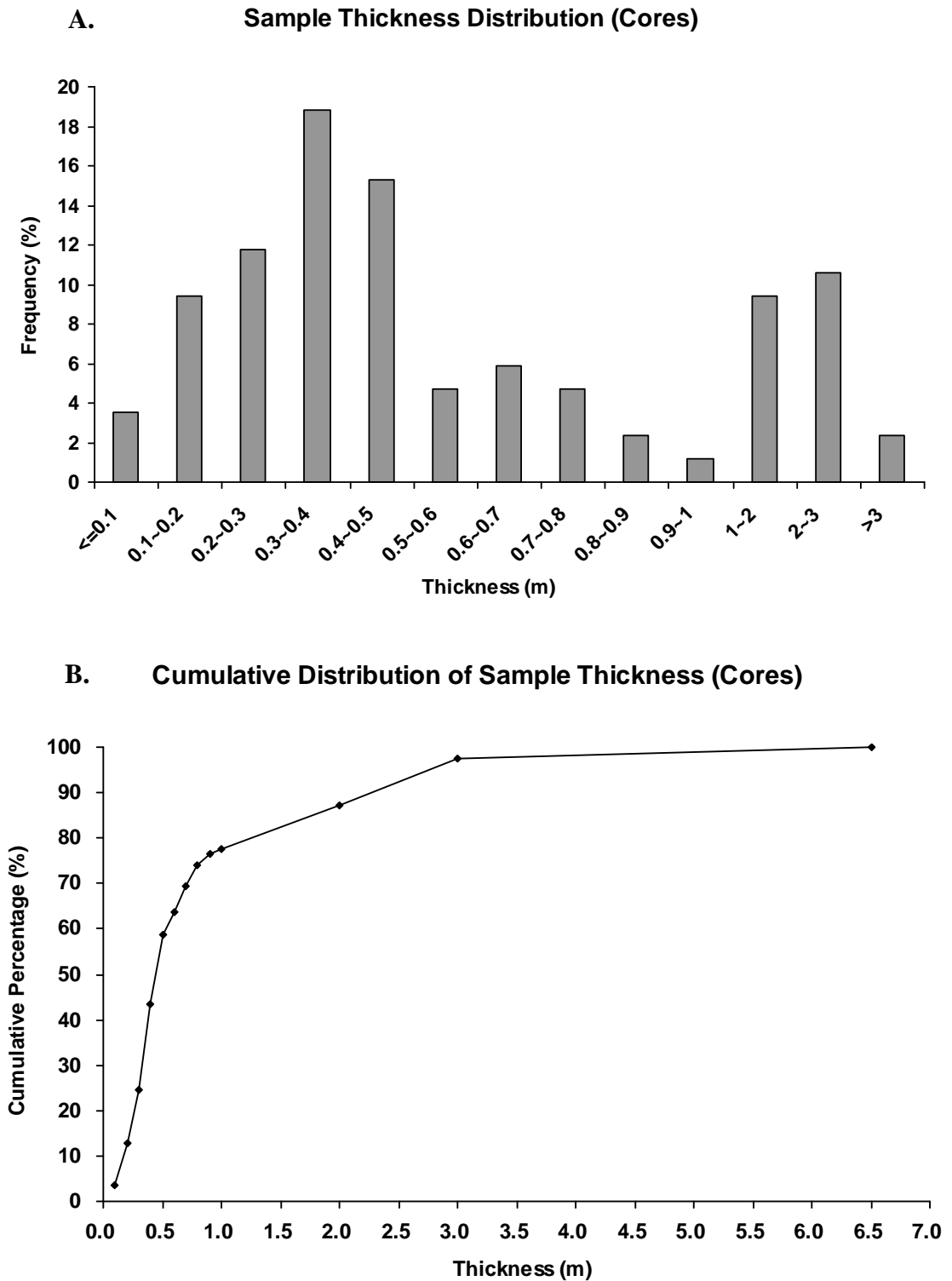
Figure 7A and 7B.   Thickness distribution of conventional ^{14}C dated samples from cores (data from Broecker et al., 1956; Brannon et al., 1957; Broecker and Kulp, 1957; McFarlan, 1961; Coleman and Smith, 1964; Nelson and Bray, 1970; Frazier, 1974; Kulp, 2000).

A. **Sample Thickness Distribution (Cuttings)**

B. **Cumulative Distribution of Sample Thickness (Cuttings)**

Figure 8A and 8B. Thickness distribution of conventional ^{14}C dated samples from cuttings (data from Broecker et al., 1956; Brannon et al., 1957; Broecker and Kulp, 1957; McFarlan, 1961; Coleman and Smith, 1964; Nelson and Bray, 1970; Frazier, 1974; Kulp, 2000).
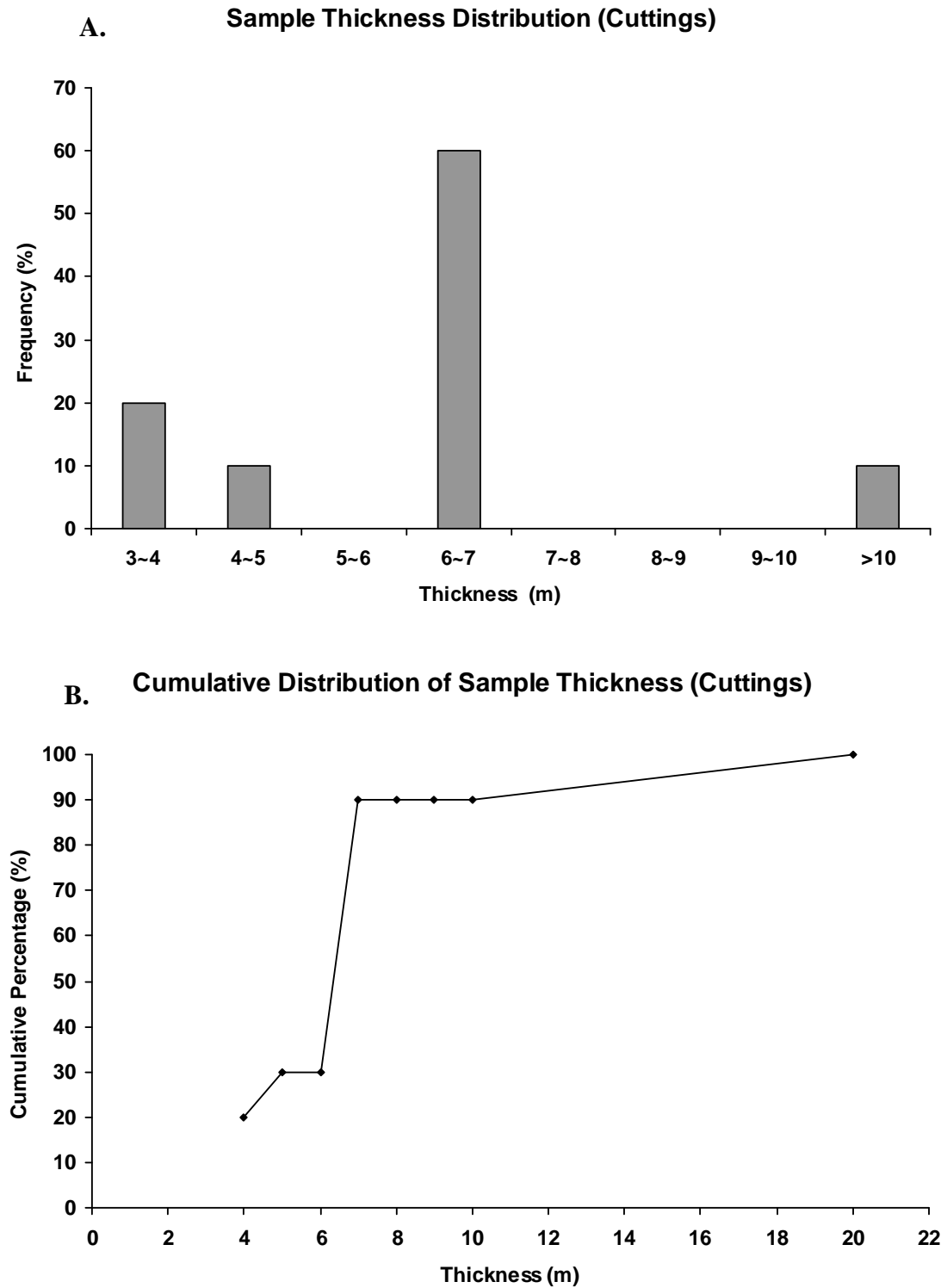
2000). According to the distribution of sample thicknesses based on these studies (Figs.

7A and 8A), I assign 1 m as thickness to conventional ^{14}C dated samples from cores and

8 m for those from cuttings. Both values are integers rounded from the 75th percentile of

the thickness distribution for cores and cuttings, repectively (Figs 7B, 8B).

2.3.3 Sampling Errors

Sampling errors arise from procedures of depth measurement, core shortening and

stretching during drilling, and non-vertical drilling (note that the latter two types of error

only apply to samples collected by coring). Some studies report sampling errors; those

errors are adopted here directly. Error estimations were made for data from studies

without information on this issue, by taking into account that sampling errors could be

significant even with high standards of cautiousness. For instance, sea-level data obtained

from a depth up to 15 m recently collected from Bayou Sale, South Louisiana, using a

Geoprobe drilling system have an average sampling error of ±10 cm including depth

measurement, core shortening/stretching and non-vertical drilling errors, using the

highest possible standards (Y.-X. Li, personal communication, 2009). Estimations are

made according to expert judgment based on contemporary studies. Under the

assumption that sea-level researchers appreciate the importance of data accuracy and

precision, a depth measurement error of ±10 cm is assigned to data from both onshore

and offshore (Kidson, 1982).

Samples from cores are rarely drilled perfectly vertically, which makes the apparent depth (D_a) of a sample larger than the true depth (D_t). The discrepancy increases with drilling depth (Fig. 9). Since the angle (θ) between D_a and D_t can be controlled within a few degrees (<5°), an error of ±1%×D_a is assigned (Engelhart, 2010).

Core shortening and stretching occur commonly, not only during rotary coring but also during hand coring. According to Morton and White (1997), up to 30% accumulated core shortening can result within a sampling interval of less than one meter; on the other hand, alternating unshortened and shortened sampling intervals are commonly observed. Thus, I assigned anaverage core shortening/stretching error of 15% of the sample depth for samples obtained by vibra-coring and rotary coring in cases that the original study did not specify a magnitude. It is believed that hand coring leads to less shortening/stretching than rotary coring (T. E. Törnqvist, personal communication, 2009) and thus should have a smaller error. Engelhart (2010) suggests a value of ±0.05 m for hand cored samples following Woodroffe (2006), in case such an error is not specified by the original study.

2.3.4 Surveying Errors

Errors from land surface elevation measurements are discussed using the following three examples that represent different approaches to obtaining the land surface elevation. All elevation data in this study are related to the North American Vertical Datum 1988 (NAVD 88).
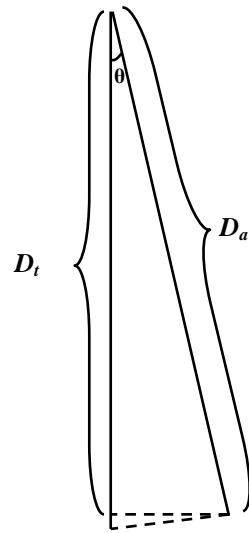
Figure 9. Illustration of non-vertical drilling. D_t and D_a represent the true and the apparent depth, respectively; θ is the borehole angle.

Ideally, researchers measure land surface elevation relative to a stable benchmark which

has an elevation well constrained with respect to a known geodetic framework (i.e.,

NAVD 88). Many studies use precise geodetic instruments for land surface surveying.

For example, Törnqvist et al. (2004a, 2004b, 2006) and González and Törnqvist (2009)

used an electronic total station and a Differential Global Positioning System (DGPS) to

survey their sampling sites and related these elevations to NAVD 88. In these studies, the

sum of errors from total station and DGPS surveying together were constrained within ±6

cm (González and Törnqvist, 2009) and ±7 cm (Törnqvist et al., 2004a; 2004b; 2006),

respectively. As demonstrated in these studies, these researchers paid great attention to

data precision, which means errors could be considerably larger. With this in mind, an

error of ±5 cm is assigned to the total station leveling and ±5 cm to DGPS surveying for

data from studies which used these high-precision surveying methods but without

providing information related to precision and errors.

Many early studies (e.g., Brannon et al., 1957; Broecker and Kulp, 1957; McFarlan, 1961;

Coleman and Smith, 1964; Nelson and Bray, 1970; Frazier, 1974) did not provide the

land surface elevation which is involved in calculating sample depth and associated errors.

In these cases, I obtained land surface elevations from topographic map information in

TOPO! 4.2. The surface elevation error is determined as one half contour interval on the

topographic map used to locate the sampling sites. For instance, topographic maps for

most sample sites in this study use a 5 ft (~1.5 m) contour interval, thus ±75 cm is

adopted as the land surface elevation error. Elevations in TOPO! 4.2 are "meters/feet

above mean sea level" instead of related to the North American Vertical Datum (NAVD)

88 datum. Thus, the MSL recorded by the nearest tide gauge would be used when

calculating sample elevation relative to NAVD 88. In cases where sample elevation is

measured from cross sections (e.g., Gould and McFarlan, 1959) the half vertical scale

interval is applied as the land surface elevation error. For instance, the vertical scale

interval is 5 ft (1.5 m) in Gould and McFarlan (1959) and hence the land surface

elevation error is ±75 cm. In these early studies, the elevation of offshore samples is

related to the water surface which is unclearly defined as "present sea level". In these

cases, I refer "present sea level" to the present MSL recorded by the nearest tide gauge

associated with an error of one half spring tidal range assigned as "tide error".

Finally, it has to be kept in mind that sampling sites might have experienced subsidence

between the collection date and the current analysis. Furthermore, local tide levels that

are used as reference water levels might have fluctuated during the same time interval.

Although it is beyond the scope of this thesis to quantitatively assess its contribution to

the total vertical error of sea-level data, it is worth taking this issue into account in future

studies.

2.4 Compaction Effects

Sediment compaction is a local effect that can cause considerable vertical displacement

of sea-level indicators and varies spatially from one site to another. In order to generate a

RSL curve with more than just local significance, the role of sediment compaction must be eliminated.

The recognition of the potentially significant contribution of sediment compaction in RSL reconstructions can be traced back to the 1960s to sea-level studies in the Netherlands (Jelgersma, 1961) and in the northeastern United States (Kaye and Barghoorn, 1964). Törnqvist et al. (2008) quantitatively estimated the magnitude of sediment compaction in the Mississippi Delta by analyzing the rate of deformation of initially horizontal peat beds, finding compaction rates up to 5 mm/yr on millennial timescales and possibly as much as 10 mm/yr on decadal to centennial timescales. A strong linear correlation between compaction rate and overburden thickness was found.

A recent study from the east coast of England (Horton and Shennan, 2009) based on a comparison of different types of peat beds (e.g., basal peat and intercalated peat) found a significant correlation between the amount of compaction and the overburden thickness as well as the total thickness of the Holocene succession. In the same study, the correlation between the compaction amount and the depth to the compaction-free basement of the peat layer was also investigated, although only one site out of six suggested a strong relationship.

Enlightened by these previous studies, attempts at similar analyses were performed with sea-level data in this thesis. Two parameters that are most likely to determine the extent

of compaction for each sea-level index point or limiting point are tabulated if relevant data are available: 1) the overburden thickness and 2) the depth to the consolidated basement. In addition, the nature of sediment facies (e.g., sediment type, grain size, organic content, and water content) over/underlying each sea-level indicator are also listed if any relevant information exists, since these factors directly or indirectly determine the extent of compaction. Instead of identifying samples as "base of basal", "basal", or "intercalated" (Shennan et al., 2000a; Engelhart, 2010), overburden thickness and depth to the consolidated basement combined with sediment facies provide a more quantitative sense of the possible extent of compaction of samples.

Although a fully quantitative correction for compaction effects would require further field and modeling studies which are not attempted here, several studies have suggested a quantitative approach to apply a compaction correction to the thickness of samples collected in sea-level studies (Van de Plassche et al., 2005; Berendsen et al., 2007). These authors discussed basal-peat samples located a few centimeters above the underlying consolidated basement and Berendsen et al. (2007) suggested correction factors of 1.5 and 2.5 for the base and top of these peat samples, respectively. For example, in order to decompact a 10 cm thick peat sample that is 5 cm from the consolidated basement, one would multiply 5 cm by 1.5 and 5+10 cm by 2.5, yielding a decompacted peat sample 7.5 to 37.5 cm above the compaction-free substrate. This correction not only enlarges the thickness of the peat sample but also elevates it. I solely performed the thickness correction and avoid any elevation change corrections which are beyond the scope of this

thesis. The maximum correction factor of 2.5 is applied to sample thicknesses based on

the reported maximum compaction amount of 60% for peat beds (Van Asselen, in press)

(2.5 = 1/(1-0.6)). This correction is carried out to obtain decompacted sample thicknesses

(Td) for both basal and non-basal peat and organic-rich sediments (e.g., humic clay).

Since most other samples in the sea-level database consist of shell materials that are

likely much less compressible, no sample thickness correction is carried out in those

cases.

Finally, a sample midpoint correction is performed for those samples with a decompacted

thickness. In these cases, the elevation of the top of the sample is obtained by adding the

decompacted sample thickness to the elevation of the base of the sample. The sample

midpoint elevation is the average of the base and the decompacted top elevations.

2.5 Age Uncertainty

2.5.1 Radiocarbon Measurement Techniques: a Brief Overview

Radiocarbon (^{14}C) atoms decay, turning into ^{14}N atoms by emitting an electron and a

positron. The decay characteristics of ^{14}C enable it to be used for radiometric dating and

the decay time is calculated as

$$t = -\frac{1}{\lambda} \cdot \ln \frac{N}{N_0} \qquad [5]$$

where t is the time of decay, λ is the disintegration constant for a given radiometric

isotope, N is the measured amount of the radiometric isotope in the sample, and N_0 is the

original amount of the radiometric isotope in the sample before it started disintegrating. This equation is only valid under the assumption that no isotopic exchange occurred between the sample and the environment after the disintegration started.

Given the half life of radiocarbon of 5568 years (Libby, 1952) the decay constant λ for ^{14}C is 1/8033. (Note that some studies use a 5730 year half life.) Since the amount of ^{14}C in the sample can be represented by 1) its abundance relative to ^{12}C or ^{13}C (i.e., the ratio ^{14}C/^{12}C or ^{14}C/^{13}C), or 2) its radioactivity (A), the disintegration equation of ^{14}C can be rewritten as

$$t_m = -8033 \cdot \ln \frac{\left(\frac{^{14}C}{^{12}C}\right)_t}{\left(\frac{^{14}C}{^{12}C}\right)_0} \qquad [6]$$

or

$$t_m = -8033 \cdot \ln \frac{A_t}{A_0} \qquad [7]$$

where t_m represents the measured ^{14}C age of the sample, subscript 0 represents age zero and subscript t corresponds to a certain time when the sample age is t. The original radioactivity or relative abundance of ^{14}C is represented by the modern activity or the modern ^{14}C/^{12}C (or ^{14}C/^{13}C) ratio of NBS (National Bureau of Standards) oxalic acid held by the American Bureau of Standards, respectively. The radiocarbon age of a sample can then be calculated if the remnant ^{14}C abundance or activity can be measured.

2.5.1.1 Conventional Radiocarbon Dating

The conventional radiocarbon dating technique involves beta (β) disintegration counting, which yields the ^{14}C age of a sample by detecting the electrically charged β particles emitted from ^{14}C decay over a period of time. The rationale behind this is that the rate of β emission reflects the residual level of ^{14}C activity in the sample (Libby, 1952; Bowman, 1990; Walker, 2005). There are two ways to perform β counting, including gas counting (if the sample is converted into CO_2) and liquid scintillation counting (if the sample is converted into benzene, C_6H_6). Gas counting became popular in the 1950s because it avoids nuclear fall-out contamination. Liquid scintillation counting has been prevailing since the 1960s, due to a reduction of the required sample amount (Bowman, 1990).

2.5.1.2 Accelerator Mass Spectrometry

Instead of counting the β emission, accelerator mass spectrometry (AMS) is used to detect the amount of ^{14}C relative to the lighter carbon isotopes (^{12}C and ^{13}C) directly by employing: 1) an accelerator to separate ^{14}C from molecules with similar weight such as ^{14}N and ^{13}CH$^+$, and 2) a magnetic field to separate the carbon isotopes which are then counted by an ion detector. AMS significantly decreases the sample size required for dating from several grams of carbon (as needed for β counting) to 1 milligram of carbon or less (Bowman, 1990; Walker, 2005).

The ^{14}C age from either β counting or AMS is not necessarily the true age of the sample. Instead, it is the mean value with a standard deviation (σ) of the normal probability

distribution resulting mainly from counting statistics (Walker, 2005). For example,

sample O-226 from McFarlan (1961) is 4840 ± 130 ^{14}C years old, which implies that the

probability is 68% for the sample age to lie between 4710 and 4970 ^{14}C years before

present.

2.5.2 Radiocarbon Dating Errors

Sources of error in radiocarbon age determination, as discussed in this thesis, include the

analytical (laboratory) error that is the standard deviation of the ^{14}C age based primarily

on the counting statistics, as well as additional non-analytical (interpretational) errors.

The non-analytical uncertainty may be caused by the specific nature of the dated material,

reservoir effects, and isotopic fractionation.

Some of the radiocarbon ages listed in the main spreadsheet of the sea-level database are

the weighted mean values of multiple samples (i.e., subsamples) calculated following

Mook and Van de Plassche (1986) as

$$\overline{t_m} = \frac{\sum\limits_{j=1} \dfrac{t_{m_j}}{E_{a_j}^{2}}}{\sum\limits_{j=1} \dfrac{1}{E_{a_j}^{2}}} \qquad (j = 1, 2, 3, \ldots) \qquad [8]$$

and the analytical error of the weighted mean age is

$$\overline{E_a} = \frac{1}{\sqrt{\sum\limits_{j=1} \dfrac{1}{E_{a_j}^{2}}}} \qquad (j = 1, 2, 3, \ldots) \qquad [9]$$

Subsample information is listed in a separate spreadsheet.

2.5.2.1 Analytical Error

The analytical error arises from a variety of sources, mainly consisting of 1) process blanks which contain small but measurable amounts of ^{14}C due to contamination during the sample preparation processes, and 2) statistical variance of the ^{14}C measurement due to both the internal "Poisson error" and the external precision of the repeatability test (Karlen et al., 1968; Olsson, 1970; Stuiver and Polach, 1977; Stuiver, 1980; Bowman, 1990). Usually radiocarbon laboratories provide the analytical error as the standard deviation. In this thesis, the analytical error is adopted directly from the studies where they were reported, except for data from a few early studies (e.g., Gould and McFarlan, 1959) where this uncertainty is not reported. A positive correlation between sample age and the laboratory error is expected: in other words, older samples have a larger analytical error.

In order to give an appropriate estimation of the analytical error for age measurements from studies that did not report analytical errors, I quantified the correlation between the ^{14}C age and the analytical error by performing a regression analysis on 116 ^{14}C measurements from contemporaneous studies that did report errors (Kulp et al., 1952; Broecker et al., 1956; Brannon et al., 1957; Broecker and Kulp, 1957; McFarlan, 1961; Coleman and Smith, 1964). A good exponential relationship between ^{14}C ages and the errors is shown in Fig. 10, following the equation
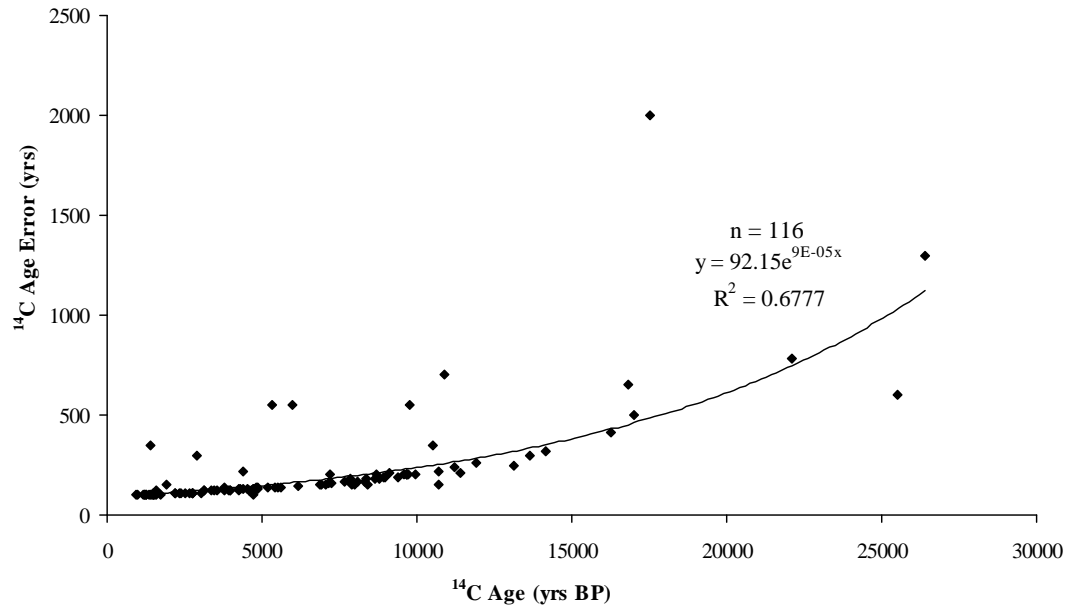
Figure 10. Exponential regression analysis of the relationship between ^{14}C age and the analytical error.

Table 3. Laboratory error estimation of ^{14}C ages up to 23000 yr BP for studies prior to the 1970s

^{14}C Age Range (yr BP)	Error Assigned (yr)
≤3000	100
3000-7000	150
7000-10000	200
10000-12000	250
12000-14000	300
14000-17000	400
17000-19000	500
19000-21000	600
21000-23000	700

$$E_a = 92.15 \cdot e^{t_m \cdot 9 \times 10^{-5}}$$ [10]

An age-error conversion table (Table 3) was then established based on Equation [10] to assign the analytical uncertainties for ^{14}C measurements from studies before the 1970s without such information (e.g., Gould and McFarlan, 1959), with error values rounded to the nearest 50 ^{14}C years.

2.5.2.2 Nature of Dated Material

Carbonaceous organic remains constitute some of the most widely used materials in radiocarbon dating for geological purposes. With respect to the accuracy of the ages provided by these materials, this category can be subdivided into bulk samples (e.g., bulk peat, mixed shells) and short-lived identifiable samples (e.g., plant macrofossils and single shells).

According to Mook and Van de Plassche (1986), contamination of bulk peat can occur in at least two ways: 1) mechanical contamination – reworking and redeposition of older organic materials which is particularly significant in sediments with low organic content; and 2) botanical contamination which in most cases involves the penetration of roots that rejuvenate the bulk ^{14}C age.

A comparison of ^{14}C ages of pairs of bulk peat and macrofossils originating from the same sample (data from Törnqvist et al., 1992) was made to evaluate the distribution of the age difference (bulk age minus macrofossil age). Based on the resulting histogram
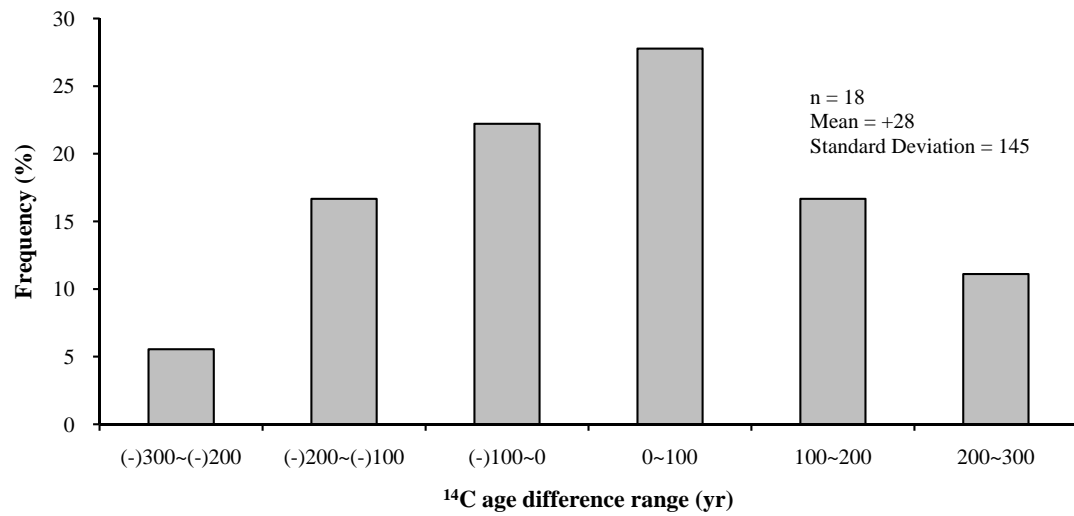
Figure 11. Distribution of ^{14}C age difference (bulk peat minus macrofossil) of bulk peat-macrofossil pairs (data from Törnqvist et al., 1992).

(Fig. 11), I assume that the "bulk minus macrofossil" value is normally distributed, with a mean of zero (the observed mean of +28 is not significantly larger), and a standard deviation of 145 ^{14}C years. On the other hand, the reported bulk peat analytical errors in this dataset have a mean value of only 70 ^{14}C years, while the reported macrofossil ages have a mean error of 80 ^{14}C years. The normal distribution suggests that mechanical and botanical contamination which influence ^{14}C ages of bulk peat in opposite ways cancel each other out in many cases. Thus, the bulk peat ^{14}C ages are still reliable and hence useful. However, an extra error to account for possible bulk peat contamination appears to be appropriate.

To test the necessity of assigning such a bulk error, a chi-square (χ^2) test was carried out. The χ^2 test yields a significance level of 98% for the necessity to assign a bulk error of ± 100 ^{14}C years ($\sqrt{145^2 - \left(70^2 + 80^2\right)}$), rounded to the nearest 10 years. Statistical test details are provided in the Appendix. The same problem can be expected when comparing bulk carbonates and individual shell specimens. Therefore, an error of ± 100 ^{14}C years is added to ^{14}C ages of bulk carbonate samples as well.

2.5.2.3 Reservoir Effect

Ocean surface water approaches carbon isotopic equilibrium with the atmosphere. After the surface water diffuses and sinks into the deep ocean, dissolved inorganic ^{14}C in the water decays without replenishment because the deep ocean water is isolated from the atmosphere for long periods of time (Walker, 2005). Thus, the ^{14}C age of marine

carbonate samples crystallized from this ^{14}C depleted ocean water (e.g., shells as discussed in this thesis) is older than the true age. This effect occurs worldwide, although it varies depending on local/regional geological and/or climatic condition (Walker, 2005). An average reservoir age of 400 ± 100 ^{14}C years is generally applied to ^{14}C ages from open marine environments (e.g., Waelbroeck et al., 2001; Hughen et al., 2004). I adopted this reservoir age for marine carbonate ^{14}C ages from the Gulf of Mexico in this thesis.

In estuarine systems along the Gulf of Mexico, however, the reservoir age is potentially greater than the global one. Radiocarbon age comparisons on wood-shell pairs from three estuaries along the Texas Coast (Fig. 12A) reveal a reservoir age increase from east to west, from 400 to 800 ^{14}C years (Fig. 12B) (Milliken et al., 2008). Since this area is reasonably comparable to our research area, I adopted 600 years as the average reservoir age for ^{14}C ages of estuarine carbonate samples in the Gulf of Mexico, with an uncertainty of ± 200 ^{14}C years. Shell samples that could be either open marine or estuarine would be assigned a reservoir age of 550 ± 250 ^{14}C years in order to cover the maximum reservoir correction range.

2.5.2.4 Isotopic Fractionation

Organic matter is depleted in rare isotopes (^{14}C and ^{13}C) relative to its source; this is known as isotopic fractionation. Biological pathways have the tendency to preferentially take up lighter carbon isotopes. Thus, a lower content of heavier carbon isotopes (i.e., ^{14}C and ^{13}C) is observed in organic matter, compared to the carbon reservoir from which
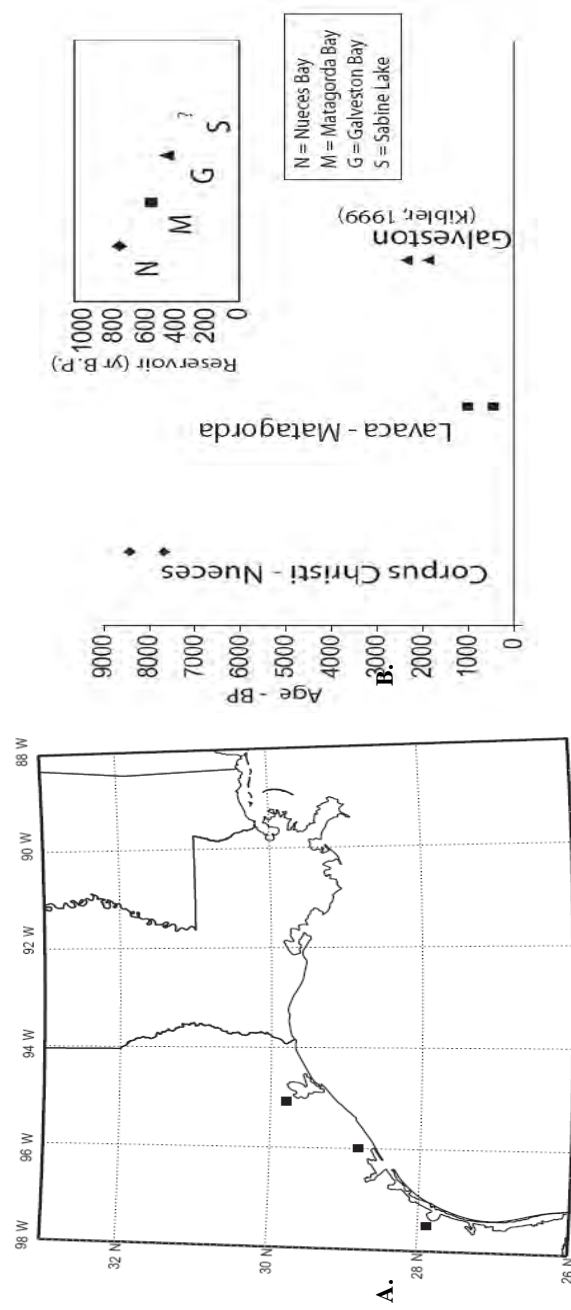
Figure 12. A. Sampling sites of wood-shell pairs (black squares). From east to west: Galveston, Lavaca – Matagorda, and Corpus Christi – Nueces; B. Reservoir effect from wood-shell pair ^{14}**C ages for each locality (Milliken et al., 2008).**

biologic carbon is obtained (Park and Epstein, 1960; Bowman, 1990). As a result, both terrestrial and marine organisms would display older ^{14}C ages if not corrected for isotopic fractionation. On the other hand, isotopic fractionation causes a systematic difference in isotopic composition of the atmospheric and oceanic carbon reservoir. The ocean preferentially absorbs heavier carbon from the atmosphere, resulting in an enrichment of ^{14}C and ^{13}C in ocean water. This effect leads to a smaller, but still noticeable, depletion of ^{14}C and ^{13}C in marine organisms (Park and Epstein, 1960). Carbonate crystallized from ocean water, however, prefers heavier carbon isotopes to the lighter ones. This characteristic combined with the heavier ocean carbon reservoir, results in marine carbonates becoming enriched in ^{14}C and ^{13}C, hence rejuvenating ages.

For these reasons, an isotopic fractionation correction is necessary to obtain accurate ^{14}C ages. According to Stuiver and Polach (1977),

$$t_m = -8033 \cdot \ln \frac{A_s}{A_{on}} \qquad [11]$$

where A_s represents the sample ^{14}C activity, and A_{on} represents the normalized (or isotopic fractionation corrected) ^{14}C activity of the standard which is directly related to the NBS oxalic acid, representing the original radiocarbon activity when the disintegration started. Then the normalized ^{14}C age, t_n, would be

$$t_n = -8033 \cdot \ln \frac{A_{sn}}{A_{on}} \qquad [12]$$

where A_{sn} represents the normalized ^{14}C activity of the sample after isotopic fractionation correction. According to Stuiver and Robinson (1974),

$$A_{sn} = A_s \cdot \frac{\left(1 + \frac{-25}{1000}\right)^{1.9}}{\left(1 + \frac{\delta^{13}C}{1000}\right)^{1.9}} \qquad [13]$$

where $\delta^{13}C$ is the measurement or the estimation of sample ^{13}C isotopic composition, defined as

$$\delta^{13}C = \left(\frac{\left(\frac{^{13}C}{^{12}C}\right)_{sample}}{\left(\frac{^{13}C}{^{12}C}\right)_{VPDB}} - 1 \right) \times 1000 \, \text{‰} \qquad [14]$$

The international $\delta^{13}C$ standard used to be the Pee Dee Belemnite (PDB) but is currently the NBS19-Limestone known as VPDB. A $\delta^{13}C$ value of -25‰ is applied to represent the no-fractionation assumption. In other words, no correction is needed if the sample $\delta^{13}C$ value is -25‰ (Stuiver and Robinson, 1974). By combining Equations [11], [12], and [13], we obtain

$$\Delta t_i = t_n - t_m = 8033 \cdot \ln \frac{A_s}{A_{sn}} = 8033 \cdot \ln \frac{\left(1 + \frac{\delta^{13}C}{1000}\right)^{1.9}}{0.975^{1.9}} \qquad [15]$$

where Δt_i represents the age difference between the uncorrected ^{14}C age and the corrected age, and hence the isotopic fractionation correction. This equation can be re-arranged as

$$\Delta t_i = 15262.7 \cdot \ln\left(1 + \frac{\delta^{13}C}{1000}\right) + 386.418 \qquad [16]$$
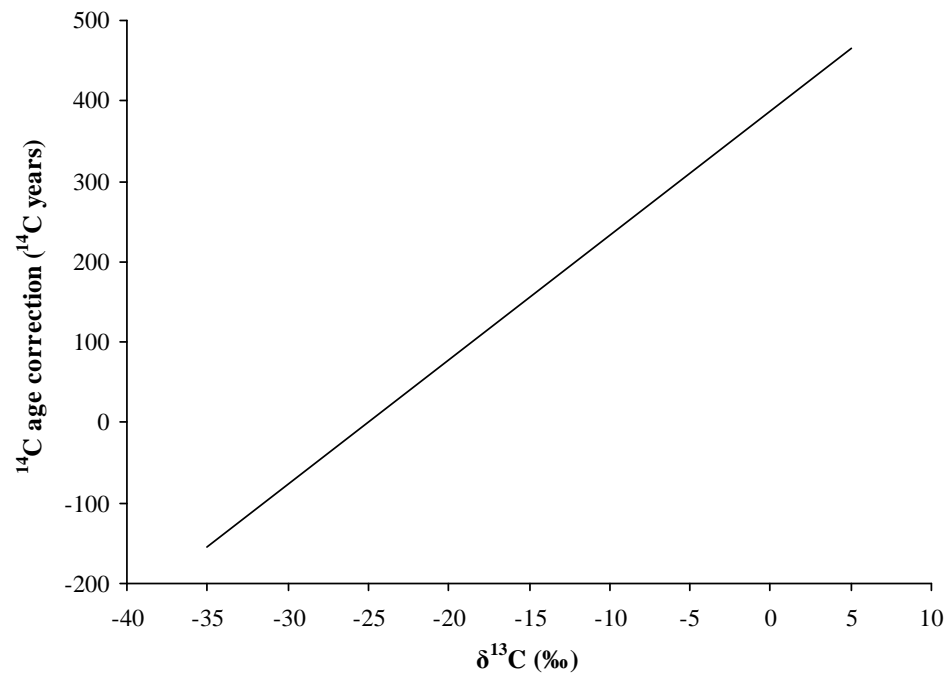
Figure 13. Isotopic fractionation correction curve based on Equation 16 for radiocarbon dated materials with δ^{13}C values ranging from -35‰ to +5‰.

Equation [16] enables us to convert the sample $\delta^{13}C$ value to the age correction value due to isotopic fractionation (Fig. 13), given that the stable isotope ^{13}C can be measured by AMS or stable isotope mass spectrometry.

The rejuvenating effects of isotopic fractionation on ^{14}C ages have been addressed by radiocarbon dating researchers since the 1950s (e.g., Craig, 1953; Rafter, 1955; Broecker and Olson, 1959). Corrections for radiocarbon measurements based on the $\delta^{13}C$ value (measured by mass spectrometry or estimated) can be traced back to the 1960s in the earliest volumes of the journal *Radiocarbon* (e.g., Barker and Mackey, 1959; Olsson, 1959; Östlund, 1959; Nydal, 1960; Tauber, 1960; Stuiver and Deevey, 1961; Dorn et al., 1962; Östlund et al., 1962; Ralph and Stuckenrath, 1962). However, the $\delta^{13}C$ correction did not become a routine procedure for every laboratory until the mid 1980s, as shown by publications from this time onwards in *Radiocarbon*. Radiocarbon laboratories made the isotopic fractionation correction routine gradually, so there is no clear time line as to the starting point of the routine correction for all laboratories.

Defining the starting point for isotopic fractionation correction for specific laboratories can be done by examining their ^{14}C measurement reports (mostly published in *Radiocarbon*). For instance, ^{14}C ages that are used in this thesis are mainly from five laboratories: Lamont Geological Observatory at Columbia University (L), Humble Oil and Refining Company (O), Shell Development Company Exploration and Production Research Division (Sh), Mobil Oil Research and Development Corporation Field

Research Laboratory (SM) and the Robert J. Van de Graaff Laboratorium at Utrecht

University, The Netherlands (UtC). Among these laboratories, Humble Oil, Shell, and

Mobil did not provide any evidence for isotopic fractionation correction and they have

been inactive since 1973, 1969 and 1977, respectively. Thus, ^{14}C measurements from

these laboratories are considered as not corrected and manual correction would apply to

these data. Lamont is one of the laboratories that discussed and carried out isotopic

fractionation correction earliest. However, the ^{14}C measurements used in this thesis were

published before 1959 when the Lamont laboratory first addressed this issue. Therefore,

these data are considered as uncorrected as well and need correction. The more recent

radiocarbon data from the Utrecht laboratory have reported $\delta^{13}C$ data and have been

corrected for isotopic fractionation so that no further correction is needed.

In cases where it is certain that no isotopic fractionation correction was performed, such a

correction, including an error assessment, was carried out in this thesis. The $\delta^{13}C$ range of

a variety of materials of interest to this study and available from the literature are listed in

Table 4. Conversion from $\delta^{13}C$ ranges of specific materials to corresponding ^{14}C age

correction ranges is based on Equation [16] (Fig. 13). The mean value of the age

correction range and its uncertainty is listed for each material. For example, for

"undifferentiated peat", the $\delta^{13}C$ range is -32 to -12‰. An age correction range of -110 to

+200 ^{14}C years would be obtained using Equation [16]. The mean value of this range is

+50 ^{14}C years, and the uncertainty for this age correction value (E_i) is ±160 ^{14}C years.

Table 4. δ^{13}C value range and age correction for different materials

Material	δ^{13}C (‰)	Δt_i (^{14}C years)
Wood [1]	-29 ~ -23	-20±50
Organic carbon-rich sedimentary material from freshwater environment [2]	-28.5 ~ -25.5	-30±20
Organic carbon-rich sedimentary material from intermediate (salinity) environment [2]	-25 ~ -18	+60±60
Organic carbon-rich sedimentary material from brackish environment [2]	-20 ~ -15	+120±40
Organic carbon-rich sedimentary material from saline environment [2]	-18 ~ -14	+140±30
Undifferentiated peat [3]	-32 ~ -12	+50±160
Estuarine and freshwater carbonates from the northern Gulf of Mexico [4]	-15 ~ +5*	+310±150
Marine carbonates [4]	-4 ~ +3	+380±50

1. (Walker, 2005); 2. (Chmura et al., 1987); 3. (Törnqvist et al., 2004a); 4. (Hoefs, 1997). *This δ^{13}C range covers fresh to saline environments.

In cases where it is unknown whether isotopic fractionation correction has been performed to the original ^{14}C measurement, an isotopic fractionation error, E_I, instead of an age correction with uncertainty, is assigned to the ^{14}C age in the sea-level database. I define this as

$$E_I = |\Delta t_i| + |E_i| \qquad [17]$$

where Δt_i represents isotopic fractionation correction for the specific dated material, and E_i represents the associated isotopic fractionation correction error. For instance, a ^{14}C measurement of an undifferentiated peat sample from Kulp (2000) is reported as 3350 ± 70 yr BP, without evidence as to whether it has been corrected for isotopic fractionation. The isotopic fractionation error is $\pm(50 + 160) = \pm 210$ ^{14}C years based on Equation [17].

2.5.2.5 Integrated Age Error

Given the above analysis, the integrated ^{14}C age correction would be

$$Age_c = t_m - \Delta R + \Delta t_i \pm E_{ta} \qquad [18]$$

where t_m represents the measured ^{14}C age, ΔR represents reservoir age, Δt_i represents isotopic fractionation correction, and E_{ta} stands for total age error which is the square root of the sum of all squared errors,

$$E_{ta} = \sqrt{E_a^2 + E_b^2 + E_r^2 + E_i^2} \qquad [19]$$

where subscripts *a, b, r, i* represent analytical, bulk, reservoir, and isotopic fractionation, respectively. In cases where it is not known if isotopic fractionation correction has been carried out

$$E_{ta} = \sqrt{E_a^2 + E_b^2 + E_r^2 + E_I^2} \qquad [20]$$

The non-analytical errors discussed above lead to larger error ranges of [14]C

measurements (especially for relatively precise measurements) when corrections are

required. Following Equations [18] and [20], the corrected ^{14}C age would be

$$3350 \pm \sqrt{70^2 + 100^2 + (50 + 160)^2} = 3350 \pm 240 \quad \text{yr BP for the example discussed above}$$

from Kulp (2000).

2.5.3 Radiocarbon Age Calibration

In this thesis, the Calib Rev 6.0.1 program (henceforth Calib, http://intcal.qub.ac.uk/calib/)

(Stuiver et al., 2005) is used to calibrate ^{14}C ages into calendar years. The Calib manual is

provided by Stuiver et al. (2005) along with the calibration software. As discussed in

Section 2.4.2, all radiocarbon measurements are corrected for a variety of errors before

calibration. Calib itself provides options to perform some of these corrections, including

1) adjustment of the laboratory error, 2) a choice of data sets and calibration curves for

different carbon reservoirs, and 3) $\delta^{13}C$ correction. The first two options are built into the

program, while a MS Excel spreadsheet for $\delta^{13}C$ correction is provided as a supplement

to the program.

Calib provides two options to increase the reported standard deviation of the radiocarbon

measurement: either by applying an error multiplier, K, or by adding a variance, f^2 (Fig.

14). The age error then would be increased to either Kσ or $\sqrt{\sigma^2 + f^2}$ (Stuiver et al.,

Figure 14. "Sample Properties" and "Calibration Option Selection" windows in Calib Rev 6.0.1. [14]C measurements and associated age uncertainties are input in the "Sample Properties" window along with other information (left window). After entering all ^{14}C samples, the user selects calibration options in the "Calibration Option Selection" window (right window). Highlighted are parameters discussed in the text.

2005), where σ represents the standard deviation of the ^{14}C age (i.e., the analytical error). In this thesis, corrections of this nature have already been carried out and thus additional errors are already included in "Age Uncertainty" in the "Sample Properties" window (Fig. 14) before calibration (see Section 2.5.2). Therefore one can either choose "Treatment of Lab Error" as a multiplier in the "Calibration Option Selection" window and assign 1 to "Laboratory Error" in the "Sample Properties" window, or choose "Treatment of Lab Error" as additional variance and assign 0 to "Laboratory Error" (Fig. 14).

In the "Sample Properties" window (Fig. 14), Calib offers different calibration data sets and calibration curves for different carbon reservoirs. The data sets IntCal09 and Marine09 (Reimer et al., 2009) are most commonly used for terrestrial samples from the Northern Hemisphere and samples from the global oceans, respectively. A global reservoir age of 405 ± 22 ^{14}C years has been used to carry out marine reservoir correction when Marine09 is chosen to calibrate ^{14}C measurements (Reimer et al., 2009). One thing that has to be kept in mind is that ΔR (with ΔR uncertainty) in the "Sample Properties" window (Fig. 14) is the site-specific offset from the global reservoir correction (405 ± 22). Since all the ^{14}C measurements of marine and estuarine carbonates in this thesis have been corrected for reservoir effects prior to calibration (see Section 2.5.2.3), I simply choose Intcal09 to calibrate all the three types of samples (terrestrial, open marine, and estuarine). The result is the same as performing the reservoir correction within Calib (Fig. 15).
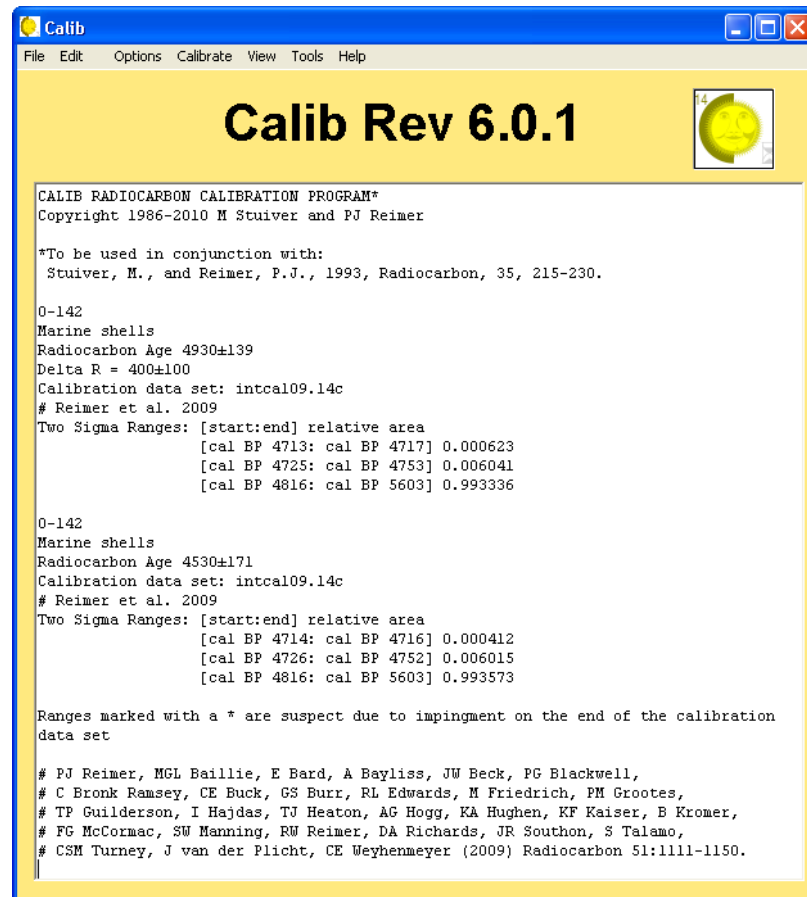
Figure 15. Calibration results of sample O-142 (marine shells) from Brannon et al. (1957) using the IntCal09 data set. Pre-correcting the ^{14}C measurement ($4530 \pm 171 = 4930\text{-}400 \pm \sqrt{139^2 + 100^2}$) and calibrating it with $\Delta R = 0 \pm 0$ yields essentially the same result compared to the built-in reservoir correction (4930 ± 139, $\Delta R = 400 \pm 100$).

Calib provides a δ^{13}C correction spreadsheet (Stuiver et al., 2005) for users to make sure

^{14}C ages are corrected for isotopic fractionation for cases where this has not yet been

done by the radiocarbon laboratory. Comparisons of calculations between the spreadsheet

and Equation [14] indicate that they give the same correction results. Again, the isotopic

fractionation correction, where necessary, has already been performed in a previous step

(Section 2.5.2.4).

Besides the correction options, Calib provides other options such as precision, unit of age

for output, sample identification, and so on ("Calibration Option Selection" window in

Fig. 14). I choose the 2σ confidence level as the precision, calendar years before present

(cal BP, 0 cal BP = 1950 AD) as the age reference frame, and either laboratory code or

sample name (for cases where the laboratory code is not available) as the sample

identification. The calibrated calendar years in the result window are rounded to the

nearest year (Fig. 15). However, this is unrealistically precise for ^{14}C ages with analytical

age errors greater than 50 ^{14}C years (Stuiver et al., 2005). Hence, I round all the

calibrated ages to the nearest 10 years as recommended by the Calib Manual.

The calibrated calendar age is highly recommended by some studies (e.g., Telford et al.,

2004) to be displayed as an age range covering the full probability distribution. This

approach is adopted here by using an error box representing each sea-level index point

where its width represents the total age error. However, for practical purposes (e.g.,

calculation of trend curves) a point of central tendency needs to be assigned within each

Calib Rev 6.0.1

```
CALIB RADIOCARBON CALIBRATION PROGRAM*
Copyright 1986-2010 M Stuiver and PJ Reimer

*To be used in conjunction with:
 Stuiver, M., and Reimer, P.J., 1993, Radiocarbon, 35, 215-230.

UtC-12503
Plant macrofossil
Radiocarbon Age 4771±31
Calibration data set: intcal09.14c
# Reimer et al. 2009
Two Sigma Ranges: [start:end] relative area
                  [cal BP 5333: cal BP 5347] 0.025848
                  [cal BP 5354: cal BP 5358] 0.004889
                  [cal BP 5369: cal BP 5370] 0.002313
                  [cal BP 5465: cal BP 5590] 0.96695

Ranges marked with a * are suspect due to impingment on the end of the calibration data set

# PJ Reimer, MGL Baillie, E Bard, A Bayliss, JW Beck, PG Blackwell,
# C Bronk Ramsey, CE Buck, GS Burr, RL Edwards, M Friedrich, PM Grootes,
# TP Guilderson, I Hajdas, TJ Heaton, AG Hogg, KA Hughen, KF Kaiser, B Kromer,
# FG McCormac, SW Manning, RW Reimer, DA Richards, JR Southon, S Talamo,
# CSM Turney, J van der Plicht, CE Weyhenmeyer (2009) Radiocarbon 51:1111-1150.
```

A.

B.

Figure 16. A, B. Example of a ^{14}C age calibration result, in tabulated and graphical format, respectively; C. sea-level index point UtC-12503 plotted as an error box with a weighted mean age (open triangle); the arithmetic mean age (filled circle) is shown for comparison.

error box. The weighted mean of the full probability distribution of the calibrated

calendar age is chosen as the central point of the total age range as recommended by

Telford et al. (2004). For example, index point UtC-12503 (Törnqvist et al., 2004a) has

multiple 2σ calibrated age ranges with highly variable probability densities (Fig. 16A, B).

The weighted mean of this age probability distribution is 5520 cal yr BP

(=0.025848×(5333+5347)/2+0.004889×(5354+5358)/2+0.002313×(5369+5370)/2+0.966

95×(5465+5590)/2) and differs by 60 years from the arithmetic mean (5460 cal yr BP) as

derived from the upper and lower limit of the 2σ calibrated age range (Fig. 16A, C).

2.6 Database Structure

The sea-level database consists of three spreadsheets, including (1) a main spreadsheet

with all sea-level index points and limiting data points, (2) a spreadsheet with subsamples

for cases where the ^{14}C age in the main spreadsheet is the weighted mean of ^{14}C

measurements of multiple subsamples, and (3) a spreadsheet with rejected data with the

reason of rejection listed. All three spreadsheets contain information with regard to the

following four aspects: geographic location, descriptive information, age, and elevation.

A set of examples is used here to illustrate this structure (Tables 5 through 10).

In order to locate any single sea-level index point or limiting data point in this database

geographically, both the general location and the decimal longitude and latitude of the

sampling sites are provided (Table 5). The general location of a single sea-level indicator

is a relevant geographic name from the region (e.g., a city or county name). The

longitude and latitude of each data point are either directly adopted or converted from the format in the original study. Both the original location data and the converted decimal longitude-latitude (long/lat) data are listed for each entry.

The descriptive information (Table 6) includes 1) a reference to the original study from which the data originate (multiple sources are listed for cases where original information has been updated or augmented in subsequent studies), 2) sample name, 3) sampling method, 4) material dated, 5) dated facies, 6) overburden facies, and 7) underlying facies. The first two entries, combined with radiocarbon laboratory code (see the following paragraph), help to identify the data point. Entries 3 and 4 contribute to determining sample thickness and sampling error. Entry 4 is also consulted when assigning the non-analytical radiocarbon dating errors. Entries 4, 5, 6 and 7 together provide qualitative information relevant to compaction effects.

The next portion of the database (Table 7) refers to age. This includes the radiocarbon laboratory code, number of subsamples, the ^{14}C age followed by the laboratory error, the bulk error, the reservoir correction and its associated error, the δ^{13}C measurement by the original study, the isotopic fractionation correction based on the nature of the dated material followed by its associated error, the corrected ^{14}C age and error, and the 2σ confidence limits of the calibrated calendar age followed by the arithmetic mean with age error, plus the weighted mean.

Data relevant to elevation can be subdivided into three parts, including the

measured/estimated elevation/depth (Table 8), the tidal data (Table 9), and the vertical

uncertainties (Table 10). The elevation-related measurements include the overburden

thickness, the depth to underlying consolidated strata, the land/water surface elevation,

depth of the top, base, and midpoint of the sample below the surface, elevation of the top,

base, and midpoint of the sample relative to the geodetic frame as defined in the original

study, followed by the sample midpoint elevation relative to the geodetic vertical datum

NAVD 88. It is worth noticing that the two columns of midpoint elevation are different if

the original geodetic frame is not with respect to NAVD 88. For instance, the midpoint

elevation of sample O-2246 (Frazier, 1974) is -0.05 m relative to MSL in the original

study. Since the nearest tide gauge shows that the present MSL is 0.32 m above NAVD

88, the sample midpoint elevation relative to NAVD 88 becomes -0.05 + 0.32 = 0.27 m

NAVD 88. The next item is paleo mean sea level relative to NAVD 88 which is

calculated based on the elevation of the sample midpoint and the reference water level.

The type and elevation of the tide level used as the reference water level for each data

point are listed right after the elevation measurement columns, followed by the National

Geodetic Survey (NGS) tide-gauge station code. The nearest tide gauge to a sampling site

is used to obtain tide levels. The subsequent entries are all the tide levels used. Following

are uncertainty entries including indicative range, indicative range error, sample thickness,

decompacted sample thickness, sampling error, core shortening/stretching error,

non-vertical drilling error, land surface surveying method and errors, and total elevation

error and uncertainty.

Table 5. Structure of the sea-level database: geographic location

General location	Latitude/Longitude - decimal degree		Latitude/Longitude – degree/minute/second		UTM Coordinates				Public Land Survey System				Descriptive location
	N	E	N	W	Zone	Northing	Easting	Datum	Township	Range	Section	Quadrant	
St. James Parish, LA	30.0640	-90.6830			15	3327.940	723.370	NAD 27					
St. Mary Parish, LA	29.6978	-91.4669			15	3286.280	648.320	NAD 83					
St. Mary Parish, LA	29.8508	-91.7318			15	3302.927	622.500	NAD 83					
Schooner Bayou Canal, LA	29.732	-92.337	29°43.9'	92°20.'									
Lafourche Parish, LA	29.309	-89.818							21 S	26 E	1	on the beach ridge in center	
Iberia Parish, LA	29.9255	-91.2158							13 S	12 E	23	2100 ft S., 1600 ft E. of NW corner	
Bayou Sale, LA	29.64	-91.54											Bayou Sale
Creole Canal, LA	29.88	-93.08											from map location
Offshore Galvesto, TX	29.643	-93.778	29°38.6'	93°46.7'									
Orleans Parish, LA	29.8587	-90.0306							14 S	24 E	89	200 ft S., 1200 ft E. of NW corner	
Orleans Parish, LA	29.9160	-90.0728							13 S	24 E	2	100 ft S., 300 ft W. of NE corner	
Jefferson Parish, LA	30.0273	-90.2787							12 S	9 E	10	500' S., 200' E. of NW corner	

Table 6. Structure of the sea-level database: descriptive information

Reference	Sample name	Sampling method	Material dated	Dated facies	Oerburden facies	Underlying facies (nearest layer)
Törnqvist et al. (2004a)	Gramercy VIII-1	Hand coring	>10 charcoal fragments	humic clay	silty clay and silt loam	Paleosol on Pleistocene deposit
Törnqvist et al. (2006)	Bayou Sale I-1	Hand coring	15 *Carex peryginum* type achenes	humic clay	mainly silty clay loam	Paleosol on Pleistocene deposit
González and Törnqvist (2009)	Patout Canal IV-1	Hand coring	charcoal fragments	peat	anthropogenic fill	Paleoso on compaction-free Holocene deposit
Frazier (1974)		boring	Brackish-marsh peat		(near surface)	marsh silty clay and peat
Brannon et al. (1957); McFarlan (1961)		boring	Wood		shoreline of the Teche delta	fine-grained sand
Kulp et al. (1952); McFarlan (1961)		core	Wood			Bay deposit
Coleman and Smith (1964)	13	boring	Peat		deltaic sediment interbedded by peat layers	
Gould and McFarlan (1959)	38-I	control boring	Organic clay and silt		organic clay and silt	mix grained sediment with oyster-reef detritus
Nelson and Bray (1970)	70	rotary core	Peat		mix grained sediment containing shell fragments	Pleistocene deposit
Broecker et al. (1956); McFarlan (1961)		core	Marine pelecypod shells		shallow shelf deposit	shallow shelf deposit
Broecker and Kulp (1957); McFarlan (1961)		core	Marine shells (mostly *Crassostrea*, *Crepidula*, *Mytilus*, and *Balanus* fragmens)		fine sand	silty clay
McFarlan (1961)		core	*Arca* shells			shallow shelf deposit

Table 7. Structure of the sea-level database: radiocarbon age and calibration

Laboratory Code	Number of sub-samples	^{14}C age (yr BP)	^{14}C error (yr)	Bulk error (yr)	ΔR (yr)	ΔR error (yr)	δ^{13}C (‰)	Isotopic fractionation correction (yr)	Isotopic fractionation error (yr)	Corrected ^{14}C age (yr BP)	Corrected ^{14}C error (yr)	Calibrated age - younger limit (cal yr BP)	Calibrated age - older limit (cal yr BP)	Calibrated age - arithmetic mean (cal yr BP)	Calibrated age error (cal yr)	Calibrated age - weighted mean (cal yr BP)
UtC-11161		5795	46	0	0	0	-19.1	0	0	5795	46	6490	6730	6610	120	6590
UtC-12505		6997	40	0	0	0	-26.7	0	0	6997	40	7730	7930	7830	100	7830
UtC-12808/ 12809	2	295	21	0	0	0	-25.4/ -25.7	0	0	295	21	300	430	365	65	370
O-2246		350	100	100	0	0		120	40	470	147	0	720	360	360	470
O-111		3550	120	0	0	0		-20	50	3530	130	3470	4150	3810	340	3810
L-125A		2900	300	0	0	0		-20	50	2880	304	2320	3830	3075	755	3040
O		7240	160	100	0	0		60	110	7300	218	7630	8580	8105	475	8120
		1000	100	100	0	0		60	110	1060	179	560	1350	955	395	990
SM-220		7840	250	100	0	0		60	110	7900	291	8060	9500	8780	720	8820
L-175E		5350	550	100	400	100		380	50	5330	570	4730	7420	6075	1345	6120
L-291B		7870	170	100	400	100		380	50	7850	227	8200	9290	8745	545	8770
O-226		4840	130	0	400	100		380	50	4820	171	5050	5920	5485	435	5540

Table 8. Structure of the sea-level database: elevation

Overburden thickness (m)	Depth to consolidated underlying strata (m)	Land/water surface elevation (m)	Depth below land/water surface - top (m)	Depth below land/water surface - base (m)	Depth below land/water surface - midpoint (m)	Sample elevation - top (m)	Decompacted sample elevation - top (m)	Sample elevation - base (m)	Sample elevation - midpoint (m)	Decompacted sample elevation - midpoint (m)	Sample elevation - midpoint (m NAVD)	Decompacted sample elevation - midpoint (m NAVD)	Paleo MSL (m NAVD)	Decompacted paleo MSL (m NAVD)
7.84	0.00	1.89	7.84	7.87	7.86	-5.95	-5.91	-5.98	-5.97	-5.94	-5.97	-5.94	-6.37	-6.34
11.56	0.00	0.27	11.56	11.58	11.57	-11.29	-11.26	-11.31	-11.30	-11.29	-11.30	-11.29	-11.70	-11.69
1.67	0.00	1.39	1.67	1.69	1.68	-0.28	-0.25	-0.30	-0.29	-0.28	-0.29	-0.28	-0.69	-0.68
0.00		0.10	0.00	0.30	0.15	0.10	0.55	-0.20	-0.05	0.18	0.26	0.49	-0.49	-0.26
1.98		0.00	1.98	2.29	2.14	-1.98	-1.52	-2.29	-2.14	-1.90	-1.91	-1.67	-2.14	-1.90
7.62		0.91			7.62				-6.71		-6.48		-6.71	
11.84		0.00	11.84	12.14	11.99	-11.84	-11.39	-12.14	-11.99	-11.77	-11.76	-11.54	-11.99	-11.77
0.41	3.90	0.32			0.41				-0.09		0.22		-0.09	
22.10	0.00	0.00	22.10	22.30	22.20	-22.10	-21.80	-22.30	-22.2	-22.05	-21.89	-21.74	-22.20	-22.05
21.03		0.00			21.03				-21.03		-20.80		-21.03	
31.70		4.27			31.70				-27.43		-27.20		-27.43	
15.24		0.00			15.24				-15.24		-15.01		-15.24	

Table 9. Structure of the sea-level database: tidal data

Tide gauge code	HAT (m NAVD)	MHHW (m NAVD)	MHW (m NAVD)	MTL (m NAVD)	MSL (m NAVD)	MLW (m NAVD)	MLLW (m NAVD)	Spring tidal range (m)	Reference water Level	Elevation of reference water level (m NAVD)
NGS8761927	0.57	0.31	0.31	0.23	0.23	0.16	0.16	0.41	(HAT+MTL)/2	0.40
NGS8761927	0.57	0.31	0.31	0.23	0.23	0.16	0.16	0.41	(HAT+MTL)/2	0.40
NGS8761927	0.57	0.31	0.31	0.23	0.23	0.16	0.16	0.41	(HAT+MTL)/2	0.40
NGS8767816	1.20	0.50	0.47	0.31	0.32	0.16	0.09	1.11	(HAT+MTL)/2	0.75
NGS8761927	0.57	0.31	0.31	0.23	0.23	0.16	0.16	0.41	MTL	0.23
NGS8761927	0.57	0.31	0.31	0.23	0.23	0.16	0.16	0.41	MTL	0.23
NGS8761927	0.57	0.31	0.31	0.23	0.23	0.16	0.16	0.41	MTL	0.23
NGS8767816	1.20	0.50	0.47	0.31	0.32	0.16	0.09	1.11	MTL	0.31
NGS8767816	1.20	0.50	0.47	0.31	0.32	0.16	0.09	1.11	MTL	0.31
NGS8761927	0.57	0.31	0.31	0.23	0.23	0.16	0.16	0.41	MTL	0.23
NGS8761927	0.57	0.31	0.31	0.23	0.23	0.16	0.16	0.41	MTL	0.23
NGS8761927	0.57	0.31	0.31	0.23	0.23	0.16	0.16	0.41	MTL	0.23

Table 10. Structure of the sea-level database: vertical errors

Indicative range (m)	Indicative range error (m)	Sample thickness (m)	Decompacted sample thickness (m)	Sampling error (m)	Core shortening/ streching error (m)	Non-vertical drilling error (m)	Land surface surveying method	Surveying error (m)	GPS error (m)	Elevation estimation error (m)	Tide error (m)	Total elevation error (m)	Total elevation uncertainty (m)
0.21	0.10	0.03	0.08	0.02		0.08	Total Station; DGPS	0.03	0.04			0.14	0.18
0.21	0.10	0.02	0.05	0.02		0.12	Total Station; DGPS	0.03	0.04			0.16	0.19
0.21	0.10	0.02	0.05	0.02		0.02	Total Station; DGPS	0.01	0.05			0.12	0.14
0.56	0.28	0.30	0.75	0.10	0.02	0.00	topo map			0.75	0.56	0.98	1.35
		0.31	0.78	0.10	0.32	0.02	topo map			0.75	0.21	0.85	1.23
		1.00	2.50	0.10	1.14	0.08	topo map			0.75	0.21	1.39	2.64
		0.30	0.75	0.10	1.80	0.12	topo map			0.75	0.21	1.97	2.34
		1.00	2.50	0.10	0.05	0.00	Cross Section Profile			0.75	0.56	0.94	2.19
		0.20	0.50	0.10	3.33	0.22	"present sea-level"			0.00	0.56	3.38	3.63
		1.00		0.10	3.15	0.21	topo map			0.75	0.21	3.26	3.76
		1.00		0.10	4.76	0.32	topo map			0.75	0.21	4.83	5.33
		1.00		0.10	2.29	0.15	topo map			0.75	0.21	2.42	2.92

Chapter 3 Testing Hypotheses about Holocene Sea-Level Change

One of the main applications of the quality-controlled sea-level database is to test

conflicting hypotheses about the Holocene RSL history in the Gulf of Mexico. A

relationship of age vs. depth extracted from Holocene basal-peat records in the

Mississippi Delta illustrates a pattern of continuous RSL rise from 10 m below present to

the present level during the past 8000 years, with the rate of RSL decreasing (Fig. 17;

Törnqvist et al., 2004a, 2006; González and Törnqvist, 2009). This has been interpreted

to result predominantly from eustatic sea-level rise prior to 7000 cal yr BP, combined

with an ongoing glacio-isostatic forebulge collapse of the Gulf Coast in response to the

melting of the Laurentide Ice Sheet (Törnqvist et al., 2004a).

According to the glacial isostatic adjustment (GIA) hypothesis, those portions of the

North American continent that were covered by ice and isostatically depressed during the

last glacial are currently rebounding. In contrast, regions at larger distance from the

former ice margin such as the US Gulf Coast experienced uplift during glaciation

followed by subsidence (forebulge collapse) (e.g., Peltier, 2004).

On the other hand, data obtained from beach ridges suggest a middle Holocene RSL

highstand up to 2 m above present mean sea level around 6000 years ago (Fig. 17; Blum

Figure 17. Comparison of sea-level index points from basal peat in the Mississippi Delta (boxes, Törnqvist et al., 2004a, 2006; González and Törnqvist, 2009) and peat (open circles) and beach ridges (solid circles) from the central Texas Coast (Blum et al., 2001).

et al., 2001) which would be at odds with the GIA hypothesis. To address this conflict, a 1-D steady-state and a 3-D visco-elastic flexural isostatic model was proposed by Blum et al. (2008) to simulate the effects of cyclic sediment loading/unloading on vertical land surface motions. These models were run under boundary conditions (i.e., 40 m for the thickness of sediments, 80 km for the valley width, and 1.8 g/cm^3 for the sediment density) constrained by the history of Lower Mississippi Valley incision and filling over the past 30,000 years, as well as estimated earth parameters (i.e., 30 km for the effective elastic thickness of the lithosphere, plus a value of 4×10^{20} Pa s for upper mantle (above 670 km depth) viscosity and 3×10^{22} Pa s for lower mantle viscosity).

Results from the 1-D elastic model indicate that a subsidence of 9 to 12 m (from the margin to the center of the valley) can be caused by the sediment loading, followed by the same magnitude of uplift resulting from sediment unloading (Fig. 18A). The 3-D viscoelastic model gives a similar magnitude of surface deflection as the 1-D model and rates of subsidence/uplift of 0.8 to 1 mm/yr (Fig. 18B). In both models, the subsidence/uplift dissipates over a distance of 100 km from the valley margin (Fig. 18A, B). Assuming that eustatic sea level had reached the present level prior to 6000 cal yr BP, the amount of subsidence caused by sediment loading in the Lower Mississippi Valley would be adequate to induce about 6 m of RSL rise as recorded by the basal-peat records.

Testing of the flexural model involves comparing sea-level index points from southwestern Louisiana >100 km away from the Mississippi paleovalley margin with
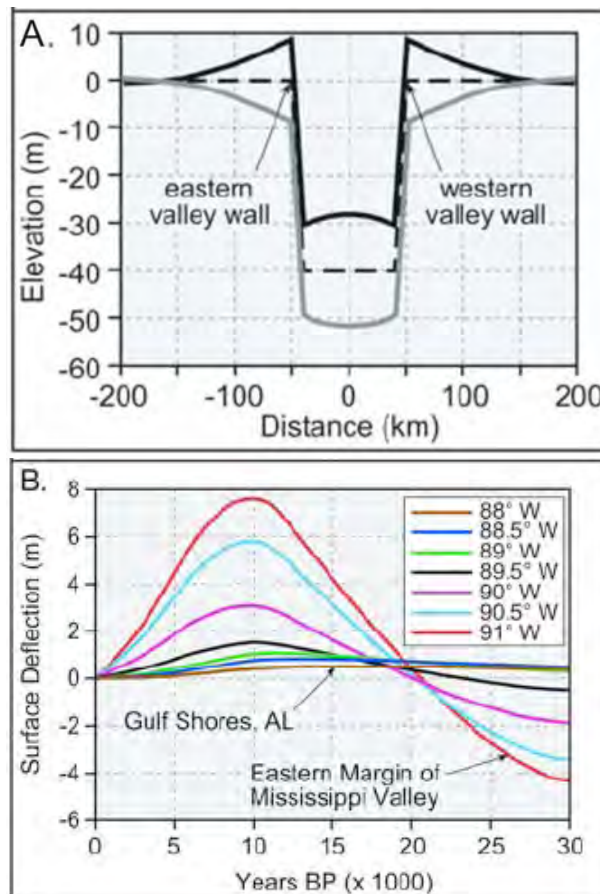
Figure 18. A.1-D flexural uplift and subsidence model. Maximum surface deflection applied to a hypothetical land surface that simulates the northern Gulf of Mexico shoreline. Dashed line approximates the Pleistocene-Holocene contact in the Lower Mississippi Valley. Black line and grey line illustrate the uplift and subsidence due to the unloading and loading by sediment, respectively. B. 3-D visco-elastic uplift and subsidence model . Plots of surface deflection through time at different locations along the Gulf of Mexico shoreline, illustrating uplift followed by subsidence in response to unloading then loading, with dissipation of the signal with distance along the shoreline (Blum et al., 2008).

RSL records from the Mississippi Delta. The idea is that if the flexural model is correct, Holocene RSL data away from the Mississippi Delta should not be subject to the subsidence induced by sediment loading and would exhibit a distinctly different trend than those from the Mississippi Delta, assuming other geologic conditions are similar. Sea-level index points used for this comparison study are basal-peat samples. Peat samples within 50 cm of the consolidated substrate are considered as "basal" here since the extent of compaction effects is believed not to be significant. Peat records from Milliken et al. (2008) do not have information about the depth to the consolidated Pleistocene basement. However it is claimed in the original study that the peat samples are basal. Thus, these data are included in this analysis.

By plotting error-estimated data of basal-peat records from previous studies in the Chenier Plain, southwestern Louisiana (Gould and McFarlan, 1959; Frazier, 1974; Milliken et al, 2008), it is found that RSL change during the past 8000 years from the area outside the realm of flexural movement is consistent with the RSL history in the Mississippi Delta as recorded by Coleman and Smith (1964), Frazier (1974), Törnqvist et al. (2004a, 2004b, 2006) and González and Törnqvist (2009) (Fig. 19). This result supports the hypothesis that the RSL rise along the Gulf of Mexico is mainly controlled by glacial isostatic adjustment.
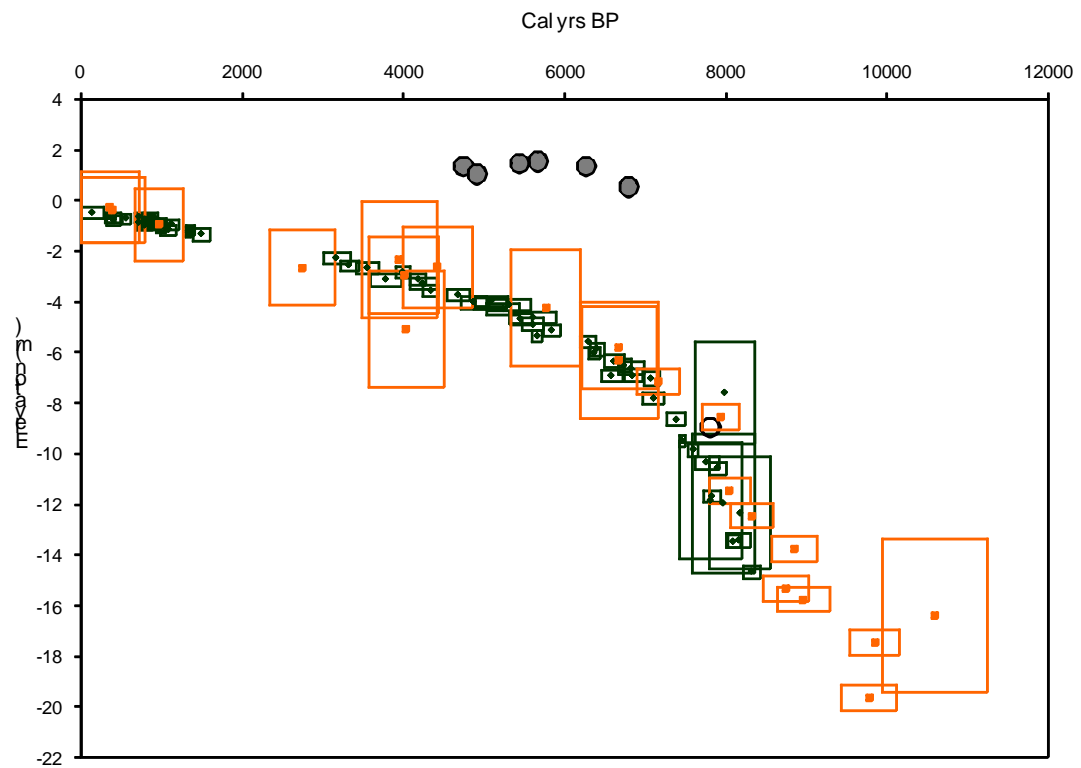
Figure 19. Comparison between basal-peat data from the Mississippi Delta (Coleman and Smith, 1964; Frazier, 1974; Törnqvist et al., 2004a, 2004b, 2006; González and Törnqvist, 2009) and the Chenier Plain (Gould and McFarlan, 1959; Frazier, 1974; Milliken et al, 2008). Black diamonds and boxes: basal-peat data from the Mississippi Delta; orange squares and boxes: basal-peat data from the Chenier Plain.

Chapter 4 Conclusions

A new sea-level database for coastal Louisiana incorporates more variables and associated error sources than previous studies, especially regarding age uncertainties (i.e., bulk error, reservoir error, and isotopic fractionation correction). The protocols proposed in this thesis should provide valuable guidelines for the construction of a standardized sea-level database for a larger region.

This new quantitative error evaluation protocol enables RSL data from different portions of coastal Louisiana to be compared, although errors are large for sea-level index points and limiting data points from early studies. Quality controlled RSL data from the Mississippi Delta cannot be distinguished from RSL records outside of the delta. This result validates that the entire area subsided in response to the glacial isostatic effects associated with the melting of the Laurentide Ice Sheet.

Appendix

The steps of the χ^2 test in detail:

Since $Age_{measured} = Age_{real} \pm Error_{analytical}$, where $Error_{analytical} \sim N(0,\sigma^2)$ (i.e. the

probability distribution of analytical error has a normal function with 0 as the mean and σ

as the standard deviation), thus

$Age_{measured} = Age_{real} \pm N(0,\sigma^2)$. In Törnqvist et al. (1992), $Age_{Bulk} = Age_{real} \pm N(0,70^2)$

and $Age_{Macrofossil} = Age_{real} \pm N(0,80^2)$. Because the real age is constant attributed to the

fact that it is the nature of the samples, we got $Age_{Bulk} - Age_{Macrofossil} = 0 \pm N(0,70^2 + 80^2)$,

i.e., $Age_{Bulk} - Age_{Macrofossil} \sim N(0,70^2 + 80^2)$ under the assumption that the bulk and

macrofossil ^{14}C age distributions are independent to each other (the rationale behind it is

that independent normal distributions $N_1(\mu_1,\sigma_1^2) \pm N_2(\mu_1 + \sigma_2^2) = N(\mu_1 \pm \mu_2, \sigma_1^2 + \sigma_2^2)$).

The calculated Bulk peat minus Macrofossil age difference follows a normal distribution

with the mean as 0 and the standard deviation as 106 years ($\approx \sqrt{70^2 + 80^2}$), implying that

both bulk peat and plant macrofossil ^{14}C ages are representative enough for the real age

of the samples, and their analytical errors (i.e. the laboratory standard deviations) are

large enough to indicate the age uncertainties. On the other hand, the observed Bulk peat

minus Macrofossil age difference is approximately a normal distribution N (28, 145^2).

Now the question is: Is it likely to obtain this observation if the Bulk peat minus

macrofossil age difference has the normal distribution as described above? In other words,

is it likely for the Bulk peat minus Macrofossil age difference to have the above normal

distribution when N (28, 145^2) is observed?

To answer the above questions, let's first make a null hypothesis (H_0): $\sigma^2 \leq 70^2 + 80^2$,

under the precondition that the Bulk peat minus Macrofossil age difference (D) has a

normal distribution N (μ, σ^2). Under H_0, each measurement of D, D_i (i: 1~18), has a

normal distribution N (μ, $70^2 + 80^2$), i.e. $D_i \sim N$ (μ, $70^2 + 80^2$). For the sample group of D,

we observed that $\sigma^2 = \dfrac{1}{18} \cdot \sum\limits_{i=1}^{18} (D_i - \mu)^2 = 145^2$. We want to know how probable a sample

group's observed $\sigma^2 \geq 145^2$ if the population's $\sigma^2 \leq 70^2 + 80^2$. In other words, we want to

know P ($\sigma^2 = \dfrac{1}{18} \cdot \sum\limits_{i=1}^{18} (D_i - \mu)^2 \geq 145^2$) =?, where P represents the probability. And a χ^2

test can give the answer.

Before performing the χ^2 test, we need a χ^2 distribution. Thus the second step is to

transform $D_i \sim N$ (μ, $70^2 + 80^2$) to a χ^2 distribution. For any normal distribution $D_i \sim N$ (μ,

σ^2), we can get $\dfrac{D_i - \mu}{\sigma} \sim N$ (0, 1). Thus for $D_i \sim N$ (μ, $70^2 + 80^2$), we get $\dfrac{D_i - \mu}{\sqrt{70^2 + 80^2}} \sim N$

(0, 1). Let $X_i = \dfrac{D_i - \mu}{\sqrt{70^2 + 80^2}}$, and $Q = \sum\limits_{i=1}^{N} X_i^2$, then

$Q = \sum\limits_{i=1}^{N} \left(\dfrac{D_i - \mu}{\sqrt{70^2 + 80^2}} \right)^2 = \sum\limits_{i=1}^{N} \dfrac{(D_i - \mu)^2}{70^2 + 80^2}$. Because each X_i (i = 1, 2, ..., N) is independent

(if each D_i is independent) and $X_i \sim N$ (0, 1), Q has a χ^2 distribution, i.e.,

$$Q = \sum_{i=1}^{N} \frac{(D_i - \mu)^2}{70^2 + 80^2} = \frac{1}{70^2 + 80^2} \cdot \sum_{i=1}^{N} (D_i - \mu)^2 \sim \chi^2(N) \text{ (in our case, N = 18). Therefore, } P$$

$$(\sigma^2 = \frac{1}{18} \cdot \sum_{i=1}^{18} (D_i - \mu)^2 \geq 145^2) = P\left(\frac{1}{70^2 + 80^2} \cdot \sum_{i=1}^{18} (D_i - \mu)^2 \geq \frac{18 \times 145^2}{70^2 + 80^2}\right) = P\left(\chi^2(18) \geq\right)$$

33.49) = 1.45%. This means, the probability to have a sample group's observed $\sigma^2 \geq 145^2$

is only 1.45%, which is statistically less probable, if the population's $\sigma^2 \leq 70^2+80^2$. And

hence, H_0 should be refused, implying that the standard deviation of 106 years for $D_i \sim N$

(μ, σ^2) is underestimated and an extra error is necessary to add on. And the next question

is: What should be added?

After rejecting the calculated value for the standard deviation of $D_i \sim N(\mu, \sigma^2)$, we can

only rely on the observed value, 145 years, at this point. Thus the distribution becomes D_i

$\sim N(\mu, 145^2)$. Let x be the extra error, then $\sigma^2 = 145^2 = 70^2 + 80^2 + x^2$. It comes out that x

$= \sqrt{145^2 - (70^2 + 80^2)} = 100$ (rounded to the nearest 10 years), which is assigned as the

bulk error to radiocarbon measurement of bulk peat.

Test of the mean of the normal distribution of Bulk peat minus Macrofossil age

differences:

Under the precondition that $D_i \sim N(\mu, \sigma^2)$, we make H_0: $\mu = 0$. Under H_0, $D_i \sim N(0, \sigma^2)$.

While the observation is $\frac{1}{18} \sum_{i=1}^{18} D_i = 28$. The question is: if the mean of the normal

distribution of D is 0, what is the probability to observe the samples' mean equal or greater than 28?

As we already proved, it is $\sigma = 145$ for $D_i \sim N (0, \sigma^2)$. Thus under H_0, $D_i \sim N (0, 145^2)$. Let

$$Y = \frac{1}{18} \sum_{i=1}^{18} D_i \text{ , thus, } Y \sim N \left(0, \frac{145^2}{18}\right). \text{ Then let's convert it to } \frac{Y-0}{\sqrt{\frac{145^2}{18}}} \sim N (0, 1). \text{ Since}$$

$$Y \geq 28, \quad \frac{Y-0}{\sqrt{\frac{145^2}{18}}} \geq 0.8193. \text{ Then } P \left(\frac{1}{18} \cdot \sum_{i=1}^{18} D_i \geq 28\right) = P \left(\frac{Y-0}{\sqrt{\frac{145^2}{18}}} \geq 0.8193\right) = 20.61\%,$$

which is statistically significant, implying that with 0 as the mean of the distribution, it is still likely to observe the samples' average equal or greater than 28.   Therefore, H_0 should not be rejected. The implication is that both bulk peat and macrofossil radiocarbon measurements represent the real age to the same extent.

List of References

Andrews, J., 1971, Sea Shells of the Texas Coast: Austin and London, University of Texas Press.

Barker, H., and Mackey, C.J., 1959, British Museum Natural Radiocarbon Measurements I: Radiocarbon, v. 1, p. 81-86.

Behrens, E.W., 1966, Recent emerged beach in eastern Mexico: Science, v. 152, p. 642-643.

Berendsen, H.J.A., Makaske, B., van de Plassche, O., van Ree, M.H.M., Das, S., van Dongen, M., Ploumen, S., and Schoenmakers, W., 2007, New groundwater-level rise data from the Rhine-Meuse delta – implications for the reconstruction of Holocene relative mean sea-level rise and differential land-level movements: Netherlands Journal of Geosciences - Geologie en Mijnbouw, v. 86, p. 333-354.

Blum, M.D., Misner, T.J., Collins, E.S., Scott, D.B., Morton, R.A., and Aslan, A., 2001, Middle Holocene sea-level rise and highstand at+2 m, central Texas coast: Journal of Sedimentary Research, v. 71, p. 581-588.

Blum, M.D., Tomkin, J.H., Purcell, A., and Lancaster, R.R., 2008, Ups and downs of the Mississippi Delta: Geology, v. 36, p. 675-678, 10.1130/g24728a.1.

Bowman, S., 1990, Radiocarbon Dating: Berkeley and Los Angeles, US, University of California Press, 64 p.

Brannon, H.R.J., Simons, L.H., Perry, D., Daughtry, A.C., and McFarlan, E.J., 1957, Humble Oil Company Radiocarbon Dates II: Science, v. 125, p. 919-923.

Broecker, W.S., and Kulp, J.L., 1957, Lamont Natural Radiocarbon Measurements IV: Science, v. 126, p. 1324-1334.

Broecker, W.S., Kulp, J.L., and Tucek, C.S., 1956, Lamont Natural Radiocarbon Measurements III: Science, v. 124, p. 154-165.

Broecker, W.S., and Olson, E.A., 1959, Lamont Radiocarbon Measurements VI: Radiocarbon, v. 1, p. 111-132.

Chmura, G.L., Aharon, P., Socki, R.A., and Abernethy, R., 1987, An inventory of ^{13}C abundances in coastal wetlands of Louisiana, USA: vegetation and sediments: Oecologia, v. 74, p. 264-271.
Coleman, J.M., and Smith, W.G., 1964, Late Recent Rise of Sea Level: Geological Society of America Bulletin, v. 75, p. 833-840.

Craig, H., 1953, The geochemistry of the stable carbon isotopes: Geochimica et Cosmochimica Acta, v. 3, p. 53-92.

Curray, J.R., 1961, Late Quaternary sea level: A discussion: Geological Society of America Bulletin, v. 72, p. 1707-1712.

Dorn, T.F., Fairhall, A.W., Schell, W.R., and Takashima, Y., 1962, Radiocarbon dating at the University of Washing ton I: Radiocarbon, v. 4, p. 1-12.

Engelhart, S.E., Horton, B.P., Douglas, B.C., Peltier, W.R., and Tornqvist, T.E., 2009, Spatial variability of late Holocene and 20(th) century sea-level rise along the Atlantic coast of the United States: Geology, v. 37, p. 1115-1118, 10.1130/g30360a.1.

Engelhart, S.E., 2010, Sea-level changes along the U.S. Atlantic coast: Implications for Glacial Isostatic Adjustment Models and current rates of sea-level change [Ph.D. thesis], University of Pennsylvania.

Frazier, D.E., 1974, Depositional -Episodes: Their Relationship to the Quaternary Stratigraphic Framework in the Northwestern Portion of the Gulf Basin: Geological Circular - Bureau of Economic Geology, the University of Texas at Austin, v. 74, p. 1-28.

González, J.L., and Törnqvist, T.E., 2009, A new Late Holocene sea-level record from the Mississippi Delta: evidence for a climate/sea level connection?: Quaternary Science Reviews, v. 28, p. 1737-1749.

Gould, H.R., and McFarlan, E.J., 1959, Geologic History of the Chenier Plain, Southwestern Louisiana: Gulf Coast Association of Geological Societies, Transactions, v. 9, p. 261-270.

Higgins, C.G., Vandendolder, E.M., Wagner, J.R., and Wilson, J.R., 2009, Topographic maps, aerial photographs, and statellite images, *in* Busch, R.M., ed., Laboratory Manual in Physical Geology: Upper Saddle River, NJ, Pearson Prentice Hall Pearson Education, Inc., p. 167-194.

Hoefs, J., 1997, Stable Isotope Geochemistry: New York, Springer Verlag Berlin Heidelberg, 201 p.

Horton, B.P., and Shennan, I., 2009, Compaction of Holocene strata and the implications for relative sea-level change on the east coast of England: Geology, v. 37, p. 1083-1086, 10.1130/g30042a.1.

Jelgersma, S., 1961, Holocene sea level changes in the Netherlands: Mededelingen van de Geologische Stichting, Serie C, v. 6, p. 1-100.

Karlen, I., Olsson, I.U., Kallburg, P., and Kilici, S., 1968, Absolute determination of the activity of two ^{14}C dating standards: Arkiv Geofysik, v. v, p. 465-471.

Kaye, C.A., and Barghoorn, E.S., 1964, Late Quaternary Sea-Level Change and Crustal Rise at Boston, massachusetts, with Notes on the Autocompaction of Peat: Geological Society of America Bulletin, v. 75, p. 63-80.

Kidson, C., 1982, Sea Level Changes in the Holocene: Quaternary Science Reviews, v. 1, p. 121-151, 10.1016/0277-3791(82)90002-6.

Kulp, J.L., Tryon, L.E., Eckelman, W.R., and Snell, W.A., 1952, Lamont Natural Radiocarbon Measurements, II: Science, v. 116, p. 409-414.

Kulp, M.A., 2000, Holocene Stratigraphy, History, and Subsidence: Mississippi River Delta Region, North-Central Gulf of Mexico [Ph. D. thesis]: Lexington, Kentucky, the University of Kentucky.

Libby, W.F., 1952, Radiocarbon Dating: Chicago, The University of Chicago Press, Chicago, Illinois, U.S.A., 124 p.

McFarlan, E.J., 1961, Radiocarbon Dating of Late Quaternary Deposits, South Louisiana: Geological Society of America Bulletin, v. 72, p. 129-158.

Milliken, K.T., Anderson, J.B., and Rodriguez, A.B., 2008, A new composite Holocene sea-level curve for the northern Gulf of Mexico: Response of Upper Gulf Coast Estuaries to Holocene Climate Change and Sea-Level Rise: Geological Society of America Special Paper 443`, p. 1-11.

Milne, G.A., and Mitrovica, J.X., 2008, Searching for eustasy in deglacial sea-level histories: Quaternary Science Reviews, v. 27, p. 2292-2302, 10.1016/j.quascirev.2008.08.018.

Mook, M.G., and Van de Plassche, O., 1986, Radiocarbon dating, *in* Van de Plassche, O., ed., Sea-level research: a manual for the collection and evaluation of data: Norwich, Geo Books, p. 525-560.

Morton, R.A., Paine, J.G., and Blum, M.D., 2000, Responses of stable bay-margin and barrier-island systems to holocene sea-level highstands, Western Gulf of Mexico: Journal of Sedimentary Research, v. 70, p. 478-490.

Morton, R.A., and White, W.A., 1997, Characteristics of and Corrections for Core Shortening in Unconsolidated Sediments: Journal of Coastal Research, v. 13, p. 761-769.

Nelson, H.F., and Bray, E.E., 1970, Stratigraphy and History of the Holocene Sediments in the Sabine-High Island Area, Gulf of Mexico, *in* Morgan, J.P., ed., Deltaic sedimentation: modern and ancient: Tulsa, Oklahoma, Society of Economic Paleontologists and Mineralogists, p. 48-77.

Nydal, R., 1960, Trondheim natural radiocarbon measurements II: Radiocarbon, v. 2, p. 82-96.
Olsson, I.U., 1959, Uppsala Natural Radiocarbon Measurements I: Radiocarbon, v. 1, p. 87-102.

Olsson, I.U., 1970, The use of oxalic acid as a standard, *in* Olsson, I.U., ed., Radiocarbon Variations and Absolute Chronology, Nobel Symposium, 12th Proc: New York, John Wiley & Sons, p. 17.

Östlund, H.G., 1959, Stockholm Natural Radiocarbon Measurements II: Radiocarbon, v. 1, p. 35-44.

Östlund, H.G., Bowman, A.L., and Rusnak, G.A., 1962, Miami natural radiocarbon measurements I: Radiocarbon, v. 4, p. 51-56.

Park, R., and Epstein, S., 1960, Carbon isotope fractionation during photosynthesis: Geochimica et Cosmochimica Acta, v. 21, p. 110-120.

Parker, R.H., 1960, Ecology and Distributional Patterns of Marine Macro-Invertebrates, Northern Gulf of Mexico, Recent Sediments, Northwest Gulf of Mexico, AAPG Special Volumes, SP 21, American Association of Petroleum Geology, p. 302 - 337.

Parker, R.H., and Curray, J.R., 1956, Fauna and bathymetry of banks on continental shelf, Northwest Gulf of Mexico: Bulletin of the American Association of Petroleum Geologists, v. 40, p. 2428-2439.

Peltier, W.R., 2004, Glabal glacial isostasy and the surface of the ice-age earth: The ICE-5G (VM2) model and GRACE: Annual Review of Earth and Planetary Sciences, v. 32, p. 111-149.

Pirazzoli, P.A., 1991, World atlas of Holocene sea-level changes: Amsterdam, Netherlands, Elsevier, 300 p.

Radiocarbon, 1980-1990,v. 22-32.

Rafter, T.A., 1955, ^{14}C variations in nature and the effect on radiocarbon dating: New Zealand Journal of Science and Technology, Section B, v. 37, p. 20-38.

Ralph, E.K., and Stuckenrath, R.J., 1962, University of Pennsylvania radiocarbon dates V: Radiocarbon, v. 4, p. 144-159.

Reimer, P.J., Baillie, M.G.L., Bard, E., Bayliss, A., Beck, J.W., Blackwell, P.G., Ramsey, C.B., Buck, C.E., Burr, G.S., Edwards, R.L., Friedrich, M., Grootes, P.M., Guilderson, T.P., Hajdas, I., Heaton, T.J., Hogg, A.G., Hughen, K.A., Kaiser, K.F., Kromer, B., McCormac, F.G., Manning, S.W., Reimer, R.W., Richards, D.A., Southon, J.R., Talamo, S., Turney, C.S.M., van der Plicht, J., and Weyhenmeye, C.E., 2009, INTCAL09 AND MARINE09 RADIOCARBON AGE CALIBRATION CURVES, 0-50,000 YEARS CAL BP: Radiocarbon, v. 51, p. 1111-1150.

Scholl, D.W., and Stuiver, M., 1967, Recent submergence of southern Florida:A comparison with adjacent coasts and other eustatic data: Geological Society of America Bulletin, v. 78, p. 437-454.

Shennan, I., 1982, Interpretation of Flandrian sea-level data from the Fenland, England: Proceedings of the Geologists's Association, v. 93, p. 53-63.

Shennan, I., 1989, Holocene crustal movements and sea-level changes in Great Britain: Journal of Quaternary Science, v. 4, p. 77-89.

Shennan, I., and Horton, B., 2002, Holocene land- and sea-level changes in Great Britain: Journal of Quaternary Science, v. 17, p. 511-526, 10.1002/jqs.710.

Shennan, I., Horton, B., Innes, J., Gehrels, R., Lloyd, J., McArthur, J., and Rutherford, M., 2000a, Late Quaternary sea-level changes, crustal movements and coastal evolution in Northumberland, WK: Journal of Quaternary Science, v. 15, p. 215-237.

Shennan, I., Lambeck, K., Horton, B., Innes, J., Lloyd, J., McArthur, J., Purcell, T., and Rutherford, M., 2000b, Late Devensian and Holocene records of relative sea-level changes in northwest Scotland and their implications for glacio-hydro-isostatic modelling: Quaternary Science Reviews, v. 19, p. 1103-1135.

Shennan, I., Peltier, W.R., Drummond, R., and Horton, B., 2002, Global to local scale parameters determining relative sea-level changes and the post-glacial isostatic adjustment of Great Britain: Quaternary Science Reviews, v. 21, p. 397-408.

Simms, A.R., Lambeck, K., Purcell, A., Anderson, J.B., and Rodriguez, A.B., 2007, Sea-Level History of the Gulf of Mexico Since the Last Glacial Maximum with Implications for the Melting History of the Laurentide Ice Sheet: Quaternary Science Reviews, v. 26, p. 920-940, 10.1016/j.quascirev.2007.01.001.

Stapor, F.W., Mathews, T.D., and Lindforskearns, F.E., 1991, BARRIER-ISLAND PROGRADATION AND HOLOCENE SEA-LEVEL HISTORY IN SOUTHWEST FLORIDA: Journal of Coastal Research, v. 7, p. 815-838.

Stuiver, M., 1980, Workshop on ^{14}C data reporting: Radiocarbon, v. 22, p. 964-966.

Stuiver, M., and Deevey, E.S., 1961, Yale natural radiocarbon measurements VI: Radiocarbon, v. 3, p. 126-140.

Stuiver, M., and Polach, H.A., 1977, Disscussion reporting of ^{14}C data: Radiocarbon, v. 19, p. 355-363.

Stuiver, M., Reimer, P.J., and Reimer, R.W., 2005, CALIB 6.0. [WWW program and documentation].

Stuiver, M., and Robinson, S.W., 1974, University of Washington geosecs north Atlantic Carbon-14 results: Earth and Planetary Science Letters, v. 23, p. 87-90.

Tanner, W.F., Demirpolat, S., Stapor, F.W., and Alvarez, L., 1989, The "Gulf of Mexico" late Holocene sea level curve: Gulf Coast Association of Geological Societies, Transactions, v. 39, p. 553-562.

Tauber, H., 1960, Copenhagen natural radiocarbon measurements III: corrections to radiocarbon dates made with the solid carbon technique: Radiocarbon, v. 2, p. 5-11.

Telford, R.J., Heegaard, E., and Birks, H.J.B., 2004, The intercept is a poor estimate of a calibrated radiocarbon age: Holocene, v. 14, p. 296-298, 10.1191/0959683604hl707fa.

Törnqvist, T.E., Bick, S.J., González, J.L., van der Borg, K., and de Jong, A.F.M., 2004b, Tracking the sea-level signature of the 8.2 ka cooling event: New constraints from the Mississippi Delta: Geophysical Research Letters, v. 31, L23309, 10.1029/2004gl021429.

Törnqvist, T.E., Bick, S.J., van der Borg, K., and De Jong, A.F.M., 2006, How Stable Is the Mississippi Delta?: Geology, v. 34, p. 697-700, 10.1130/G22624.1.

Törnqvist, T.E., De Jong, A.F.M., Oosterbaan, W.A., and Van der Borg, K., 1992, Accurate dating of organic deposits by AMS ^{14}C measurement of macrofossils: Radiocarbon, v. 34, p. 566-577.

Törnqvist, T.E., González, J.L., Newsom, L.A., van der Borg, K., de Jong, A.F.M., and Kurnik, C.W., 2004a, Deciphering Holocene Sea-Level History on the U.S. Gulf Coast: A High-Resolution Record from the Mississippi Delta: Geological Society of America Bulletin, v. 116, p. 1026-1039, 10.1130/B2525478.1.

Törnqvist, T.E., Wallace, D.J., Storms, J.E.A., Wallinga, J., Van Dam, R.L., Blaauw, M., Derksen, M.S., Klerks, C.J.W., Meijneken, C., and Snijders, E.M.A., 2008, Mississippi Delta subsidence primarily caused by compaction of Holocene strata: Nature Geoscience, v. 1, p. 173-176, 10.1038/ngeo129.

Van Asselen, S., 2010, The contribution of peat compaction to total basin subsidence: implications for the provision of accommodation space in organic-rich deltas: Basin Research, *in press*

Van de Plassche, O., 1982, Sea-level change and water-level movements in the Netherlands during the Holocene: Mededelingen Rijks Geologische Dienst, v. 36, p. 1-93.

Van de Plassche, O., 1986, Introduction, *in* Van de Plassche, O., ed., Sea-level research: a manual for the collection and evaluation of data: Norwich, Geo Books, p. 1-26.

Van de Plassche, O., Bohncke, S.J.P., Makaske, B., and van der Plicht, J., 2005, Water-level changes in the Flevo area, central Netherlands (5300-1500 BC): implications for relative mean sea-level rise in the Western Netherlands: Quaternary International, v. 133, p. 77-93, 10.1016/j.quaint.2004.10.009.

Waelbroeck, C., Duplessy, J.C., Michel, E., Labeyrie, L., Paillard, D., and Duprat, J., 2001, The timing of the last deglaciation in North Atlantic climate records: Nature, v. 412, p. 724-727. Walker, M., 2005, Quaternary Dating Methods: West Sussex, UK, John Wiley & Sons Ltd, 286 p.

Woodroffe, S.A., 2006, Holocene relative sea-level changes in Cleveland Bay, North Queensland, Australia, Durham University.

Biography

Ping Hu started her study and research pursuing a Master's degree of Science at Tulane University since the Fall 2006. She spent four and half years to finish this program under the advice and help of her Advisor, Dr. Torbjörn Törnqvist and other faculty members in the Department of Earth and Environmental Sciences. In these four years, Ping strengthened her knowledge of Earth Science by successfully finishing courses and gained experiences of field work such as sampling sediment using hand coring, navigation using geographic/topographic maps and Global Position System, and land surface surveying using Total Station leveling system. She also became skilled at using scientific analytical applications such as MS Excel, ArcGIS, Calib, TOPO, etc. by finishing her Master's thesis of a database construction about the Holocene sea-level history along the Louisiana Gulf Coast. The four and half-year academic life at Tulane also helps Ping, who is an international student, to improve her communication skills in English.